Metabolic and Population Profiles of Active Subseafloor Autotrophs in Young Oceanic Crust at Deep-Sea Hydrothermal Vents

Sabrina M. Elkassas,[a,b,#] Caroline S. Fortunato,[c,d] Sharon L. Grim,[a] David A. Butterfield,[e] James F. Holden,[f] Joseph J. Vallino,[c] Christopher K. Algar,[g] Lisa Zeigler Allen,[h,i] Benjamin T. Larson,[c,j] Giora Proskurowski,[e,k] Emily Reddington,[c,l] Lucy C. Stewart,[f,m] Begum Topçuoğlu,[f,n] and Julie A. Huber[a,#]

[a]Department of Marine Chemistry and Geochemistry, Woods Hole Oceanographic Institution, Woods Hole, MA, USA

[b]Department of Earth, Atmospheric, and Planetary Sciences, Massachusetts Institute of Technology, Cambridge, MA, USA

[c]Ecosystems Center, Marine Biological Laboratory, Woods Hole, MA, USA

[d]Present address: Department of Biology, Widener University, Chester, PA, USA

[e]Cooperative Institute for Climate, Ocean & Ecosystem Studies, University of Washington, Seattle, WA, USA

[f]Department of Microbiology, University of Massachusetts Amherst, Amherst, MA, USA

[g]Department of Oceanography, Dalhousie University, Halifax, Nova Scotia, Canada

[h]Scripps Institution of Oceanography, University of California, San Diego, La Jolla, CA, USA

[i]Department of Microbial and Environmental Genomics, J. Craig Venter Institute, La Jolla, CA, USA.

[j]Present address: Department of Biological Sciences, Renssalaer Polytechnic Institute, Troy, NY, USA

[k]Present address: MarqMetrix, ThermoFisher Scientific, Seattle, WA

[l]Present address: Great Pond Foundation, Edgartown, MA, USA

[m]Present address: New Zealand Association of Scientists, Wellington, NZ

[n]Present address: Bristol, Myers, Squibb, Summit, NJ, USA

Running Head: RNA-SIP of microbial autotrophs at hydrothermal vents

[#]Address correspondence to Sabrina Elkassas, elks@mit.edu and Julie Huber, jhuber@whoi.edu

Sabrina Elkassas and Caroline Fortunato contributed equally to this work. Julie Huber, the final author listed, is the Principal Investigator on this project.

ABSTRACT

At deep-sea hydrothermal vents, magmatically driven rock-water reactions in the crust generate energy that subseafloor microorganisms use for chemolithoautotrophy. In this study, microbial autotrophs from three diffuse hydrothermal vents at Axial Seamount in 2013 and 2014 were isotopically labeled using RNA Stable Isotope Probing (RNA-SIP), targeting subseafloor autotrophic mesophiles (30°C), thermophiles (55°C), and hyperthermophiles (80°C). We constructed taxonomic and functional profiles of active chemolithoautotrophs, examined population distributions across sites, and linked primary producers to their specific metabolic strategies within the subseafloor community. Dominant autotrophs exhibited hydrogen-dependent dissimilatory metabolisms such as sulfur and nitrate reduction and methanogenesis, as well as microaerophilic sulfide oxidation even at 80°C, consistent with fluid chemistries at each site. While hydrogenotrophic methanogenic archaea such as *Methanothermococcus* were restricted in their distribution and activity, hydrogenotrophic sulfur and nitrate reducers from the Aquificota (*Thermovibrio*), Campylobacterota (Nautiliaceae, *Hydrogenimonas*, and Desulfurobacteriaceae) were consistently active and present at all sites and years at both the population and community levels. Hydrogenase transcripts were significantly differentially expressed, and diverse hydrogenases were found in metagenome-assembled genomes of Aquificota members,

highlighting the importance and versatility of their hydrogen utilization strategies which likely contribute to their cosmopolitan distribution across geochemically disparate subseafloor sites. Together, this study provides new insights into the functional dynamics and distribution of key subseafloor autotrophic microbial communities in young oceanic crust at deep-sea hydrothermal vents.

Keywords: deep-sea hydrothermal vents, RNA-SIP, chemolithoautotrophy, diffuse flow

IMPORTANCE

Deep-sea hydrothermal vents are hotspots for life in the dark ocean, where rich animal ecosystems are supported by microbial primary producers utilizing the abundant chemical energy supplied by high-temperature water-rock reactions. Despite increasing knowledge about the geochemistry and microbiology of deep-sea hydrothermal vents, there is still a gap in our understanding of the key microbial players who fix much of the carbon at these sites, especially in the productive subseafloor. In this study, stable isotope probing was used to label active microbial autotrophs in diffuse venting fluids from 3 sites over 2 years and was combined with metatranscriptomic sequencing to identify their specific metabolic strategies. This research highlights the microbial community composition, function, gene regulation, and population dynamics that enable hydrothermal ecosystems to persist.

INTRODUCTION

Deep-sea hydrothermal systems span large temperature and geochemical gradients, from cold, oxidized seawater to hot, highly reduced hydrothermal fluid produced by rock-water reactions. There is a wide diversity of microbial niches at deep-sea hydrothermal vents, many of which are powered by chemolithoautotrophy, including chimneys, animals, venting fluids, hydrothermal plumes, mats, and the subseafloor (1). Mixing zones at and below the seafloor can

be sampled through diffuse flow vents (~5-120°C), providing a glimpse into the subseafloor habitat within oceanic crust, one of the most productive microbial niches in the vent environment (2-11). Phylogenetic, metagenomic, and metatranscriptomic studies of diffuse flow microbial communities have expanded our knowledge on the composition and variability of these communities over time and space, considering tectonic setting, host rock type, and geochemistry (e.g. 1, 7-10, 12-22). These studies show that mixing zones support taxonomically and functionally diverse microorganisms, including a mix of seawater, seafloor, and subseafloor communities that inhabit temperatures from 2°C to near 100°C across a wide range of geochemical gradients, making it difficult to pinpoint which microbes are active in the subseafloor, especially in the warmer, deeper portions of the subseafloor. However, the recent application of stable isotope probing (SIP) is providing new insights into microbial activity in the dynamic and hard-to-access subseafloor environment (8, 11, 23-24), including RNA Stable Isotope Probing (RNA-SIP).

RNA-SIP is an experimental technique by which isotopically labeled substrate is added to environmental samples at near-natural conditions, incubated, and the label incorporation is probed at the genetic level through sequencing of transcripts (8, 25-26). Resulting RNA-SIP metatranscriptomes reveal the identity and functional attributes of the microbes that incorporate the labeled substrates in each community under defined experimental conditions (8, 25-26). The first application of this method to deep-sea ecosystems was at Axial Seamount, an active deep-sea volcano on the Juan de Fuca Ridge in the northeast Pacific Ocean, where in 2013, Marker 113 diffuse fluid was incubated at mesophilic, thermophilic, and hyperthermophilic temperature regimes to reflect subseafloor conditions (8). Results revealed shifts in dominant taxa, metabolisms, and carbon fixation pathways across the temperature spectrum when compared to the unmanipulated fluid. The method was later used at multiple hydrothermal vent sites along the

93 Mariana back-arc, where thermophilic RNA-SIP incubations found that Campylobacterota were
94 active and present at all but one sampled vent, which had a high abundance and activity of
95 Aquificota. These differences were attributed to variation in hydrothermal activity due to
96 underlying tectonic setting (23). This method was also carried out *in situ* at Axial using a novel
97 instrument to complete the RNA-SIP experiment on the seafloor. Comparison of shipboard and
98 seafloor incubations at 55°C found that thermophilic, autotrophic Campylobacterota that oxidized
99 hydrogen coupled with nitrate reduction were dominant in all experiments, but transcripts for
100 thermal stress proteins were significantly more abundant in the shipboard experiments (24).

101 Building on a legacy of microbiological and geochemical studies at Axial Seamount and
102 hydrothermal systems elsewhere, we expand on these studies to include 2 years of RNA-SIP data
103 from 3 diffuse vent sites at 3 temperatures to examine how the dominant microbial subseafloor
104 autotrophs at Axial Seamount vary with temperature, fluid chemistry, geology of the vent (sulfide
105 vs. basalt), space, and time. This study contributes new *in situ* oxygen data as well as an expansive
106 metatranscriptomic dataset that enabled differential expression analysis of transcripts across
107 temperatures within and among vents, and over time. We determined the specific geochemical and
108 thermal conditions under which autotrophic communities and populations are active and identified
109 potential competition amongst these microbial groups for electron acceptors and donors, including
110 oxygen, nitrate, and hydrogen. Overall, these findings expand our knowledge of the distribution
111 and energy acquisition strategies of active microbial assemblages in the productive deep-sea
112 hydrothermal vent subseafloor at a mid-ocean ridge spreading center.

113 **RESULTS**

114 Marker 113, Anemone, and Marker 33 were chosen for sampling in this comparative study
115 because they are situated among three different vent fields within the Axial caldera, and are

geochemically and microbiologically distinct (10, 27-28; Fig S1). Chemical characteristics of all diffuse vents are shown in Table 1 and Table S1 that include data from both previously published work as well as new oxygen data collected with an *in situ* probe (10, 28; Figs 1 and 2, Table S2).

Marker 113 vent is located on top of a lava pillar at the edge of a collapse zone within an inflated lobate basalt flow. Fluids migrate up through the lava pillar and exit diffusely, resulting in wide areas on the upper surface covered with vent biota. Marker 33 is located near the eruptive fissures that fed the 1998 and 2011 eruptions, both of which covered the Marker 33 vent site. There are no high-temperature vents directly adjacent to Marker 113 or Marker 33. The nearest high-temperature vents are in the International District vent field located 0.6 km northeast of Marker 113 and 0.8 km south of Marker 33. Previous work (28) estimated the end-member hydrogen and methane concentrations feeding Marker 113 and Marker 33 vents using extrapolated chloride end-members for those two vents and the average high-temperature fluid compositions for those chloride concentrations (Table S1, Fig S2). In contrast, Anemone vent is part of a flat, actively growing sulfide mound fed by a high-temperature source fluid that diffuses through sulfide minerals and exits through very small, hot vent orifices with weak flow, with end-member fluid within a meter of the diffuse flow site sampled. At all three locations, the high-temperature source fluid can be compared with the paired diffuse flow fluid samples to infer changes in chemistry that occur in the shallow subseafloor within the basalt and/or sulfide mineral matrix.

There are clear differences in temperature and chemical composition among the three diffuse vents in this study (Fig 1, 2, Table 1). All of the venting sites are depleted in oxygen relative to near-bottom seawater in the Axial caldera (31 µmol/kg, +/- 2µmol/kg, n=24), and a linear regression of the recorded sample temperature and *in situ* oxygen concentration indicated oxygen behaves differently at each site, with zero oxygen predicted at 33°C for Marker 113 and at 52°C

for Marker 33 (Fig 1), while oxygen data from Anemone points to zero oxygen at temperatures greater than 100°C. Additional biologically relevant chemical constituents for both the diffuse fluids and the closest high-temperature end-member vent for each diffuse vent were plotted against Mg to examine deviations from conservative mixing as potential evidence of microbial activity in the venting fluids (Fig 2). At Marker 113 and 33, nitrate (Fig 2A) and H_2 (Fig 2B) were depleted and CH_4 concentrations were elevated (Fig 2C). At Anemone, there was evidence for depletion of H_2 (Fig 2B), and this site also had the highest H_2S concentrations in both years compared to the other two sites (Table 1).

	Seawater	Anemone high-temperature vent	Anemone diffuse vent	Anemone diffuse vent	Marker 33 subseafloor estimated source	Marker 33 diffuse vent	Marker 33 diffuse vent	Marker 113 subseafloor estimated source	Marker 113 diffuse vent	Marker 113 diffuse vent
Year	2015		2013	2014		2013	2014		2013	2014
Depth (m)	1520	1542.8	1542	1539		1516	1514		1520	1518
Temperature (°C)	2	232.4	28.2	20.3	340	27.3	18.5	340	24.5	24.3
pH	7.8	4.3	5.5	5.1	4	5.5	5.6	3.3	6.2	5.8
NO_3^- (µmol/kg)	39	0	35.5	35.2	0	18.3	28.2	0	7.2	8.1
H_2 (µmol/kg)	0.002	360	13.9	27.7	300	1.5	1.5	950	1.4	1
H_2S (µmol/kg)	0	7400	1036	964.7	n.d.	545	262	n.d.	729	556
CH_4 (µmol/kg)	0.002	205	14.8	31.7	70	19	6.4	56	16.9	38
Mg (mmol/kg)	52.4	0	46.5	45.6	0	45.9	48.1	0	50.2	48.8
O_2 (µmol/L)	31	0	14.4	17.6	0	14.7	23.3	0	7	9.9
Cl^- (µmol/L)	541	315	513	518	390	520	526	100	521	518
Percent Seawater	100	3.3	88.9	87	0	87.7	91.9	0	96	96.4
Microbial cells mL^{-1}	2.4×10^4		4.1×10^5	1.7×10^5		4.2×10^5	3.9×10^5		4.6×10^5	6.8×10^5

n.d. = no data

Table 1. Measurements of chemical species and microbial cell counts for diffuse vent sites Anemone, Marker 33, and Marker 113 from 2013-2014. Percent seawater was extrapolated using magnesium as a conservative tracer: $[Mg]_{vent}/[Mg]_{seawater} \times 100$, and background seawater Mg concentration at 1500m was 52.4 mmol/kg.

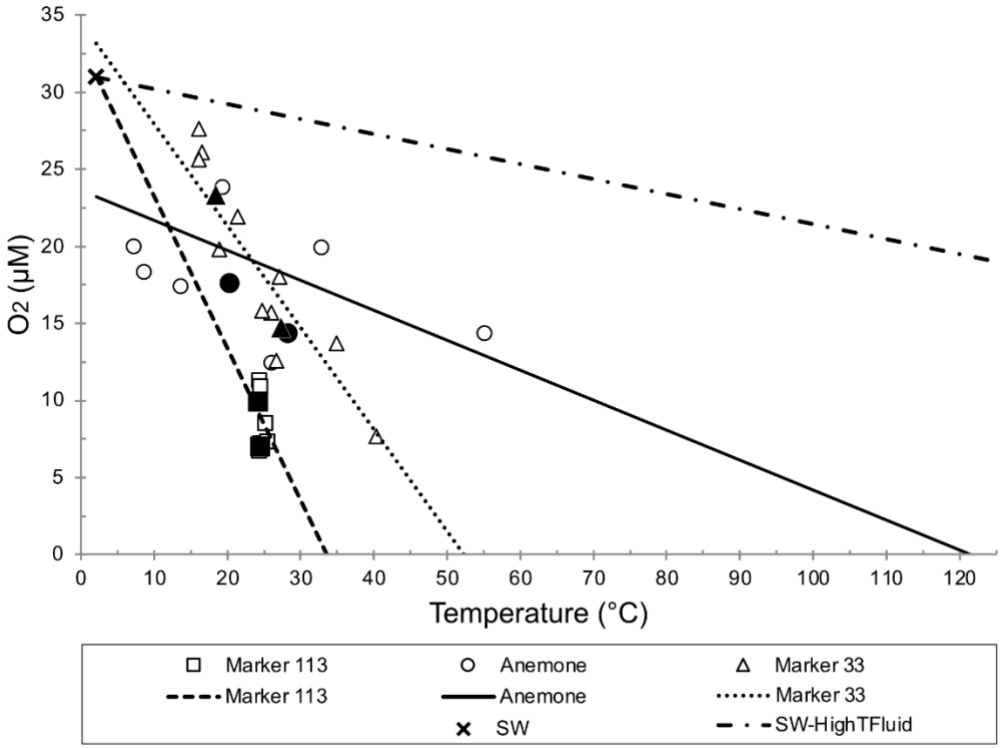

Figure 1. Figure 1. *In situ* oxygen versus temperature for diffuse vents sampled for this study. Near-bottom seawater averages 31 µmol/kg (+/- 2.2). Linear regression lines are drawn for each of the 3 vent sites for the 2 years sampled, including the ambient seawater point in the regression. The top dashed line is between seawater and a hypothetical zero-oxygen end-member at 325°C. Solid data points indicate the exact fluid sampling bag used in the SIP experiment.

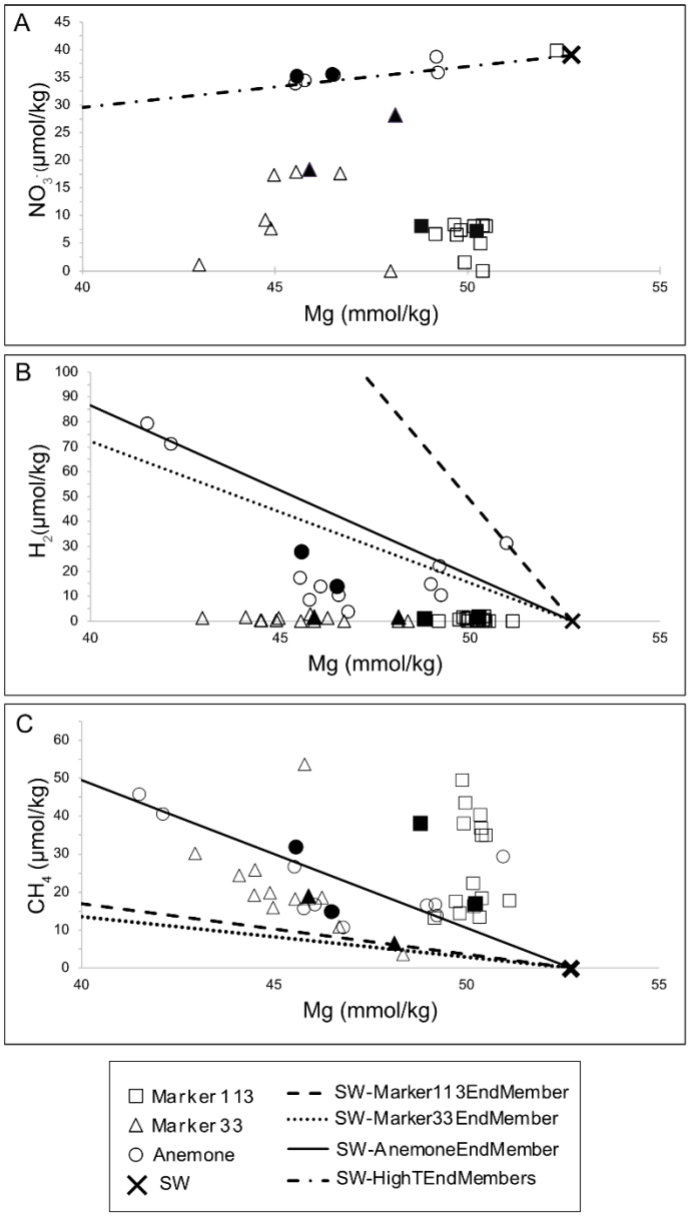

Figure 2. Vent chemical species measured at diffuse vent sites Marker 113, Anemone, and Marker 33 in 2013 and 2014. Regression lines are drawn from seawater to end-member fluid concentration for each vent and chemical species to represent conservative mixing between seawater and the high-temperature fluid for **A.** NO_3^-. All vent end-members had 0 NO_3^-, so the single regression line is between a 0 Mg/0 NO_3^- end-member and seawater. **B.** H_2 and **C.** CH_4 concentrations. Solid data points indicate the exact fluid sampling bag used in the SIP experiment.

169 *RNA-SIP experiments*

170 In total, 15 sets of RNA stable isotope probing experiments were carried out in 2013 and 2014
171 using fluids collected from Marker 113, Anemone, and Marker 33 (Table 2; Tables S3-S5).
172 Successful RNA-SIP experiments showed a heavier buoyant density peak of RNA in the ^{13}C-
173 labeled experiment compared to the ^{12}C-labeled control, indicating uptake of labeled carbon into
174 RNA (Fig S3-S5). To determine which of the 12 fractions collected should be sequenced, the
175 highest RNA concentration was chosen from the ^{12}C-light and ^{13}C-heavy peaks. If the experiment
176 had two RNA peaks, both fractions were sequenced (Marker 113 at 30 and 80°C, Fig S3C and
177 S5C). For experiments that had two time points, the ^{12}C-light and ^{13}C-heavy peaks from both time
178 points were sequenced. Corresponding ^{13}C-light and ^{12}C-heavy fractions were also sequenced as
179 additional controls. Including technical sequencing replicates, this resulted in 84 total
180 metatranscriptomes (46 ^{13}C-heavy and ^{12}C-light and 38 ^{13}C-light and ^{12}C-heavy), totaling over a
181 billion high-quality reads from paired-end Illumina sequencing. Real-time quantitative Reverse
182 Transcription Polymerase Chain Reaction (qRT-PCR) was subsequently carried out to normalize
183 data across experiments using 16S rRNA copies, as shown in Figures S3-S5. In most cases, the
184 highest concentration of RNA corresponded to the highest rRNA copy number. As described in
185 the Methods and Supplementary Methods, RNA-SIP metatranscriptomes were annotated and
186 compared with the paired metagenome and metatranscriptome generated from unmanipulated
187 diffused fluids that were filtered and fixed on the seafloor.

Vent	Year	30 °C	55 °C	80 °C
Marker 113	2013	36 hr	36 hr	18 hr*
Marker 113	2014	n.d.	18 hr, 36 hr	9 hr
Anemone	2013	n.d.	n.d.	18 hr*
Anemone	2014	24 hr, 36 hr	18 hr, 36 hr	18 hr
Marker 33	2013	36 hr	36 hr	36 hr
Marker 33	2014	24 hr, 36 hr	18 hr, 36 hr	9 hr, 18 hr

n.d. = no data; * = 1 L LVWS sample

188 **Table 2**. RNA-SIP experiments conducted, showing vent name, year, temperature of experiment, and
189 time points collected during incubation.

190 *Taxonomic composition of unmanipulated fluids and RNA-SIP experiment microbial communities*

191 The unmanipulated fluid metatranscriptomes represent the taxa with detectable transcripts at
192 the instant of sampling via filtration and immediate RNALater fixation on the seafloor. The
193 taxonomy of *in situ* active microbial community members as well as those in RNA-SIP
194 experiments was acquired by mapping non-rRNA transcripts to taxonomically classified
195 metagenomic contigs and then normalizing the genera in each sample to 100% (Fig 3A-D). The
196 taxonomy of the unmanipulated fluids was compared to both the ^{12}C-light and ^{13}C-heavy RNA-
197 SIP taxonomy, but results will focus on the ^{13}C-heavy experimental fraction, as it represents the
198 population of isotope-enriched (active) microbes.

199 All genera active at 30°C in the RNA-SIP experiments were also identified in the
200 unmanipulated fluids (Fig 3A). When comparing across all three sites at 30°C, most of the active
201 community was comprised of members of the Campylobacterota. *Sulfurimonas* transcripts were
202 observed at all three vents but were most abundant at Marker 113 (52%) and Marker 33 (31.3%)
203 (Fig 3B). Transcripts of *Cetia* (16.8-33.2%) and *Caminibacter* (12.5-22.2%) were found only in

204 RNA-SIP experiments from Anemone. At Marker 33, transcripts belonging to *Hydrogenimonas*
205 (34.3%) were more abundant compared to the other vents.

206 Like the 30°C experiments, all genera active at 55°C in the RNA-SIP experiments were
207 also identified in the unmanipulated fluids (Fig 3A). Across all three sites at 55°C, the major
208 differences in taxonomy compared to the 30°C RNA-SIP experiments were a shift to higher
209 relative abundance of *Cetia, Caminibacter, Nautilia,* and *Hydrogenimonas* transcripts, rather than
210 *Sufurimonas* transcripts (Fig 3C). Transcripts from *Caminibacter, Cetia, Nautilia*, and
211 *Hydrogenimonas* dominated in experiments from Marker 113 and Marker 33, but in 2013, these
212 experiments also had transcripts for thermophilic methanogens. *Methanothermococcus* comprised
213 17.3% and 18.6% of the 2013 active community transcripts at Marker 113 and Marker 33
214 respectively and were completely absent at Anemone in 2014, where both timepoints of 55°C
215 experiments were like those at 30°C, except for the absence of *Sulfurimonas* (Fig 3C). Further, the
216 active population at Anemone in 2014 had the same Campylobacterota taxa as seen at Marker 113
217 and 33 at 55°C.

218 Unlike at 30°C and 55°C, where Campylobacterota were abundant in both SIP
219 experiments and unmanipulated fluids, many active taxa at 80°C were in low abundance in the
220 unmanipulated fluids (Fig. 3A), including those from Phylum Aquificota and *Methanotorris* at
221 Marker 113, *Phorcysia* at Anemone, and *Thermovibrio* at Marker 33. The major differences in
222 taxonomy in the 80°C RNA-SIP experiments across sites included a higher abundance of
223 methanogenic groups at Marker 113 and 33, the presence of *Aquifex* only at Anemone, and
224 persistent detection of *Desulfurobacterium* and *Thermovibrio* at all sites and years. In the Marker
225 113 experiments at 80°C in 2013 (Fig 3D), close to half of all transcripts were from
226 hyperthermophilic methanogens, including *Methanocaldococcus* (37.6%) and *Methanotorris*

227 (2.5%). Methanogenic groups were not detected in the ^{13}C-heavy fraction in 2014 at Marker 113.
228 Hyperthermophilic methanogens were also observed at Marker 33 in 2014, along with a large
229 proportion of transcripts classified to Aquificota, including the genera *Phorcysia, Thermovibrio,*
230 and *Desulfurobacterium*. Transcripts for these genera were also abundant at Marker 113 in 2014,
231 when methanogen transcripts were absent (Fig 3D).

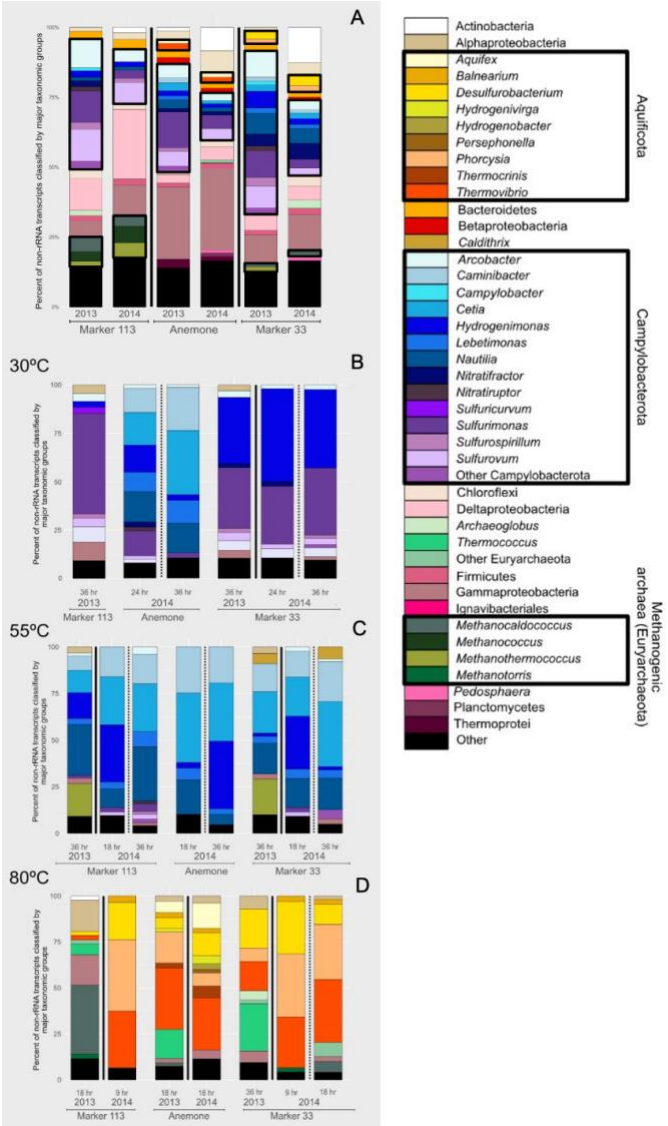

232

233 **Figure 3.** Relative abundance of major taxonomic groups of **A**. Annotated non-rRNA transcripts from
234 unmanipulated fluid metatranscriptomes and annotated non-rRNA transcripts from RNA-SIP experiments
235 at **B**. 30°C, **C**. 55°C, and **D**. 80°C.

236 *Metagenome assembled genomes (MAGs)*

237 Binning of the co-assembly of all unmanipulated diffuse fluid metagenomes resulted in 391
238 MAGs, with 120 bins remaining after filtering for quality (completeness ≥70%, contamination
239 ≤10% based on the presence of single copy bacterial and archaeal marker genes) (Table S6). These
240 bins were further filtered to remove known heterotrophs and representatives solely sourced from
241 the plume, background, or 2015 metagenomes, resulting in 25 bins. The final 11 MAGs from
242 genomic binning from all diffuse fluid metagenomes were selected based on having >4% of their
243 coding genome expressed (length of expressed genes(bp)/genome length (bp), Fig 4, Tables S6,7)
244 in any individual RNA-SIP ^{13}C-heavy fraction. The taxonomy of the highly transcribed MAGs
245 was similar to the ORF transcript taxonomy assignments (Figs 3, 4), including groups primarily
246 from the Campylobacterota, methanogens, and Aquificota.

247 Both Marker 113 and Marker 33 had *Sulfurimonas* populations (bin 41) transcribed at 30°C
248 (Figure 4), corresponding to the higher abundance of *Sulfurimonas* transcripts observed at these
249 vents (Figure 3). Two bins classified as *Hydrogenimonas* (bins 102 and 104) were transcribed
250 across different temperatures and vents. Bin 102 was transcribed only at Marker 33 at 30°C, but at
251 55°C, bin 102 was transcribed at all vents in at least one timepoint. Bin 104 transcripts, however,
252 were observed only at 30°C at Anemone. Nautiliaceae bin 340 transcripts were ubiquitous at 55°C
253 at nearly all sites and years. *Methanothermococcus* bin 335 transcripts were found at 55°C at only
254 Marker 113 and Marker 33 in 2013, while no methanogen populations were transcribed at
255 Anemone (Figures 3, 4).

256 In general, MAGs expressed a higher proportion of their coding genomes in the 80°C
257 experiments, compared to the other temperatures. *Thermovibrio* bins (bin 320 and bin 374) were
258 transcribed across all 80°C experiments, matching the high abundance of the genus in the

transcripts at all vents (Figs 3, 4). The Desulfurobacteriaceae bin 324 was transcribed in 2014 at all sites at 80°C. Aquificales bin 285, however, was restricted to only Anemone (Fig 4).

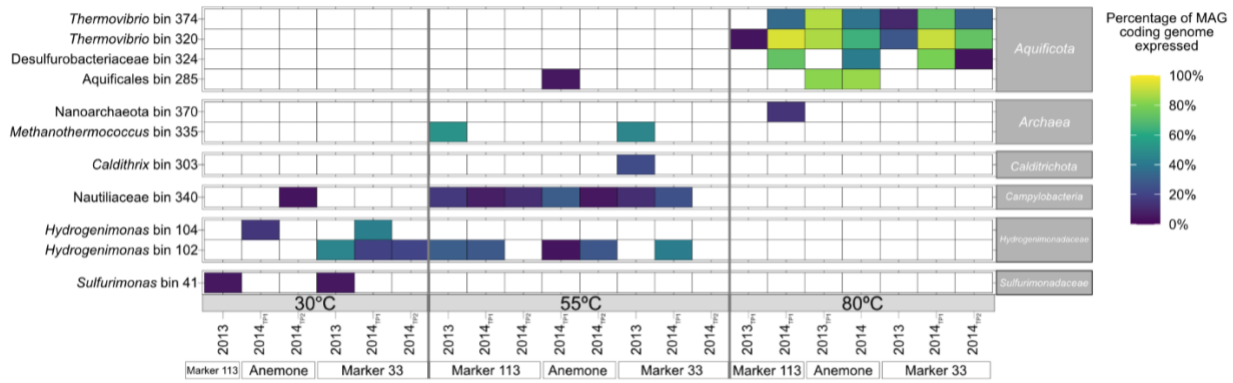

Figure 4. Metagenome Assembled Genomes (MAGs) selected based on having >4% of coding genome expressed in 30, 55 and 80°C RNA-SIP experiments. Percent of coding genome expressed = length of expressed genes(bp)/genome length (bp).

Functional attributes of active autotrophs

To determine how autotrophs in the RNA-SIP experiments acquired energy while taking up labeled inorganic carbon, we identified transcripts for key genes involved in oxygen, nitrogen, methane, hydrogen, sulfur, and carbon metabolic pathways, and compared those to the unmanipulated fluid metatranscriptomes (Fig 5, Table S8). There were similarities in major energy acquisition pathways across all sites and samples, but in each year and temperature the three vent sites differed in magnitude of transcription. Transcripts for the selected metabolic marker genes were present in most of the unmanipulated fluid metatranscriptomes (Figure 5), whereas some genes were transcribed in RNA-SIP experiments only at certain temperatures and vents, reflecting specific metabolisms being carried out by distinct subseafloor autotrophic populations under different temperature regimes. We also examined the 30 most abundant transcripts at each RNA-SIP experimental temperature (Fig S6), some of which were metabolic genes that we note here,

277 while other transcripts were related to information processing, replication and repair, and signaling
278 and cellular processes (Fig S6).

279 Transcripts for aerobic oxidative phosphorylation gene *aa*$_3$-type cytochrome c oxidase
280 (*cox*) and microaerophily gene *cbb*$_3$-type cytochrome c oxidases (*cco*) were highest in the 30°C
281 RNA-SIP experiments as compared to 55 and 80°C (Figure 5). Normalized counts of *cco* peaked
282 in Marker 33 at 30°C in both 2013 and 2014 (7,593–9,608 TPM), attributable to taxa
283 *Aliarcobacter*, *Hydrogenimonas*, *Sulfuricurvum*, *Sulfurimonas*, and *Sulfurovum* (Table S9).

284 Genes for nitrate reduction and complete denitrification were highly transcribed in almost
285 all RNA-SIP experiments (Fig 5). Of those genes, *napA*, periplasmic nitrate reductase, was the
286 most abundant transcript across all conditions. It was also one of the 30 most transcribed genes at
287 80°C (1,394–15,195 TPM) (Fig 5, Fig S6), belonging to the genera *Phorcysia* and *Thermovibrio*
288 within the Aquificota. Marker 113, and to a lesser extent, Marker 33, had transcription of genes
289 for dissimilatory nitrate reduction to ammonia (DNRA, *nirAB* and *nrf*, TPMs 8,131–16,106), and
290 these transcripts were uniquely attributed to *Sulfurospirillum* (Table S9).

291 Of the six sulfur marker genes selected, *psr* and *phs* are most functional in anaerobic
292 conditions and *sox* in aerobic conditions (29). However, many sulfur metabolism genes can
293 function across diverse oxic conditions, as they catalyze both anaerobic sulfate reduction and the
294 reverse process, sulfur-compound oxidation (30, 31). Anemone had the highest H_2S concentrations
295 as well as transcription of genes related to sulfur metabolism compared to the other two vents
296 (Table 1). For example, *sqr* had high transcription at 80°C (up to 9,695 TPM from *Aquifex*,
297 *Hydrogenivirga*, and *Phorcysia*), whereas at both Marker 113 and Marker 33, *sqr* was transcribed
298 only at the lower temperatures, 30°C and 55°C (Fig 5). The highest transcription of
299 polysulfide/thiosulfate reductase genes *psr* and *phs* occurred at 55°C in all experiments, with

300 transcripts reaching 27,947 TPM from *Hydrogenimonas*, *Cetia*, and *Nautilia* (Figure S6). While
301 *sox* transcripts were present in unmanipulated fluids at all 3 vents, activity of this gene in the RNA-
302 SIP experiments was highest in 2014 at Marker 33 at 30°C (6396 TPM) from *Hydrogenimonas*,
303 *Sulfurovum*, and *Sufurimonas* (Table S9).

304 The selected marker genes for hydrogenotrophic and acetoclastic methanogenesis were
305 transcribed in the unmanipulated fluid samples from Marker 113 and Marker 33 but were overall
306 absent at Anemone (Figure 5). Transcription of methanogenic metabolic genes was highest in
307 RNA-SIP experiments at Marker 113 in 2013 at 55°C and 80°C (up to 56,765 TPM), and Marker
308 33 at 55°C in 2013 and at 80°C in 2014 (up to 47,489 TPM). These transcripts were attributed to
309 *Methanothermococcus* and *Methanococcus* at 55°C and *Methanotorris* and *Methanocaldococcus*
310 at 80°C. Methanogenic genes *hdrA2* and *mcrA* at 55°C and *frhA*, *fwdB*, *fmdB*, and *mcrAC* at 80°C
311 were among the 30 most transcribed genes in these temperatures (Figure S6).

312 The five chosen hydrogenase marker genes were in all unmanipulated fluid
313 metatranscriptomes (Fig 5). Notably, throughout all sites and all years, 80°C RNA-SIP
314 experiments transcriptional profiles did not have quinone-reactive Ni-Fe hydrogenase *hydAB,*
315 responsible for transferring electrons from H_2 to terminal electron acceptors oxygen, nitrate,
316 sulfate, fumarate, and metals. Transcripts for *hydAB* in the 30°C and 55°C experiments belonged
317 to diverse Campylobacterota, predominantly *Sulfuricurvum* (22,883 TPM, Table S9), but also
318 *Sulfurimonas*, *Nautilia*, and *Hydrogenimonas*. Other hydrogen metabolic marker genes, such as
319 sulfhydrogenase, energy converting (*ech*) hydrogenase and Ni-Fe hydrogenase (group 1; *hya*, *hyb*),
320 were in higher abundances at 55°C and 80°C compared to 30°C and associated with *Thermococcus*
321 and Phylum Aquificota (Table S9). F420-non-reducing hydrogenase (*mvh*, *vhu*, *vhc*) used by
322 methanogens was primarily at Marker 113 and 33 at 55°C and 80°C. Quinone-reactive Ni-Fe

323 hydrogenases h*ydAB* (30°C and 55°C, Marker 33), Ni-Fe hydrogenase 1B-type *hyaC* (all vents at
324 55°C), and hydrogenase 2 large subunit *hyaB, hybC* (all vents at 80°C) were among the top 30
325 genes transcribed in the respective temperatures in the dataset (Figure S6).

326 Across all experiments and temperatures, most of the carbon fixation was via the reductive
327 tricarboxylic acid (rTCA) cycle (Fig 5). All vents at 30°C and 55°C had high transcription of rTCA
328 cycle marker genes attributed to Campylobacterota (Table S9), whereas at 80°C in both years at
329 Anemone and in 2014 at Marker 113 and Marker 33, rTCA transcripts were attributed to
330 Aquificota (Fig 5, Table S9). Eight genes involved in the rTCA/TCA cycles were in the 30 most
331 abundant genes transcribed at each temperature (Fig S6). In general, at higher temperatures when
332 methanogens were active, transcripts for the reductive acetyl-coA (Wood-Ljungdahl) pathway
333 were also abundant. For example, Wood-Ljungdahl pathway genes (*coo, acs*) attributed to
334 *Methanocaldococcus* had the highest transcription in 80°C experiments at Marker 113 (2013) and
335 Marker 33 (2014; Table S9).

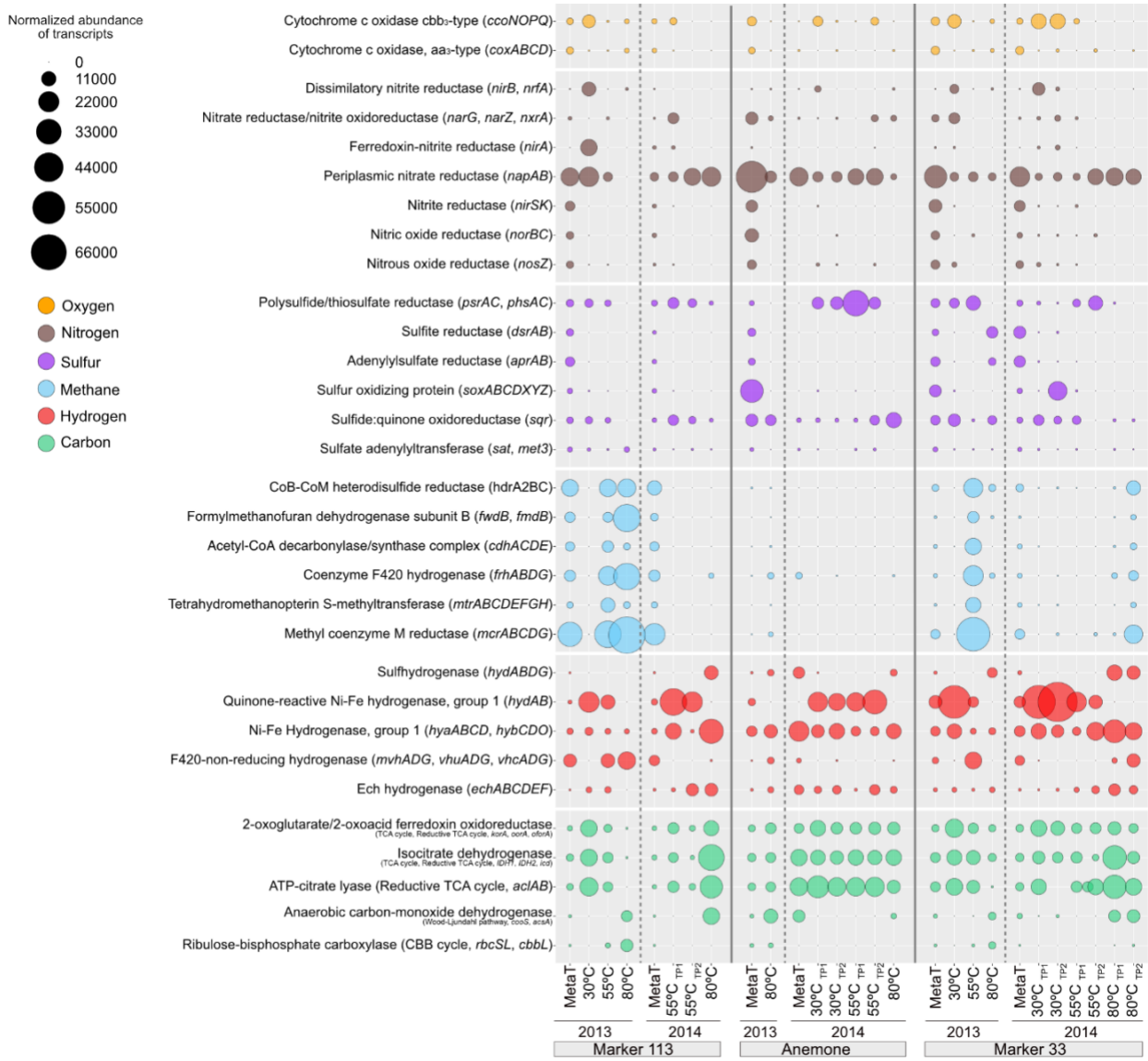

Figure 5. Normalized abundance of non-rRNA transcripts annotated in the unmanipulated diffuse fluid metatranscriptomes and RNA-SIP metatranscriptomes for key marker genes involving oxygen, nitrogen, sulfur, methane, hydrogen, and carbon metabolism. Bubble sizes represent the transcripts per million reads (TPM) attributed to each marker gene.

Differential Expression Analysis of Transcripts

Differential expression analyses using the RNA-SIP ^{13}C-heavy transcriptional profiles were conducted to determine statistical differences in transcription across experimental conditions. Depending on the hypotheses and conditions, expression profiles were compared to baseline

346 ‘expected’ transcription calibrated to the specific condition (see Methods). Across the RNA-SIP
347 dataset, 656 unique transcripts were observed to be significantly differentially expressed (SDE)
348 1520 times with an adjusted p-value of <0.05 (Table S10). Only transcripts that had a padj < 10^{-3}
349 and $\log_2$ fold-change ≥ |2| will be discussed.

350 *Differential expression across temperatures within the same vent*

351 Comparing across temperatures within the same vent resulted in the highest number of
352 significantly differently expressed transcripts (483 unique genes SDE 1030 times, Fig 6, Table
353 S11). At Marker 113, annotated transcripts with the greatest differences in expression across
354 temperatures included gene transcripts for hydrogenases, nitrate reduction, motility, heat shock,
355 and carbon metabolism (Figure 6A). Overall, as RNA-SIP experimental temperature increased,
356 the differentially expressed hydrogenase transcripts shifted from quinone-reactive Ni-Fe
357 hydrogenases (*hydAB*) at 30°C and 55°C to Ni-Fe hydrogenase (group 1) (*hya*, h*yb*) at 80°C. Heat
358 shock proteins also differed with each temperature regime, with *grpE* and *cbpA* upregulated at
359 55°C and *clpC* upregulated 80°C.

360 At Anemone, transcribed genes with the greatest differences in abundance across
361 temperatures included transcripts related to hydrogenases, methane and nitrogen metabolism,
362 carbon fixation, energy metabolism, and signaling and cellular processes (Figure 6B). Like at
363 Marker 113, there was an upregulation of quinone-reactive Ni-Fe hydrogenases (*hyd*) at 30°C and
364 55°C and Ni-Fe hydrogenases (group 1) (*hya*, *hyb)* at 80°C. There was also a similar trend for heat
365 shock proteins. At all temperatures at Anemone, where oxygen is present at temperatures of 100°C
366 or greater, all transcripts involved in oxygen-sensitive methanogenesis (*mvh*, *vhu, vhc; frh*, *fdh*,
367 and *hdr*) were downregulated.

Marker 33 had more differentially expressed transcripts across temperature than the other vents, representing genes related to hydrogenases, methane metabolism, carbon fixation, heat shock, and signaling and cellular processes (Figure 6C). Like the other two sites, Marker 33 had upregulation of oxygen-tolerant quinone-reactive Ni-Fe hydrogenases *(hydAB)* at 30°C and 55°C and oxygen-sensitive Ni-Fe hydrogenases (group 1) (*hya, hyb)* at 80°C. Heat shock proteins *grpE*, *cbpA, dnaK*, and *HSPA9* were downregulated at 80°C. Transcripts for methanogenesis were downregulated at both 55°C and 80°C, but *fdh* was upregulated at Marker 33 at 30°C.

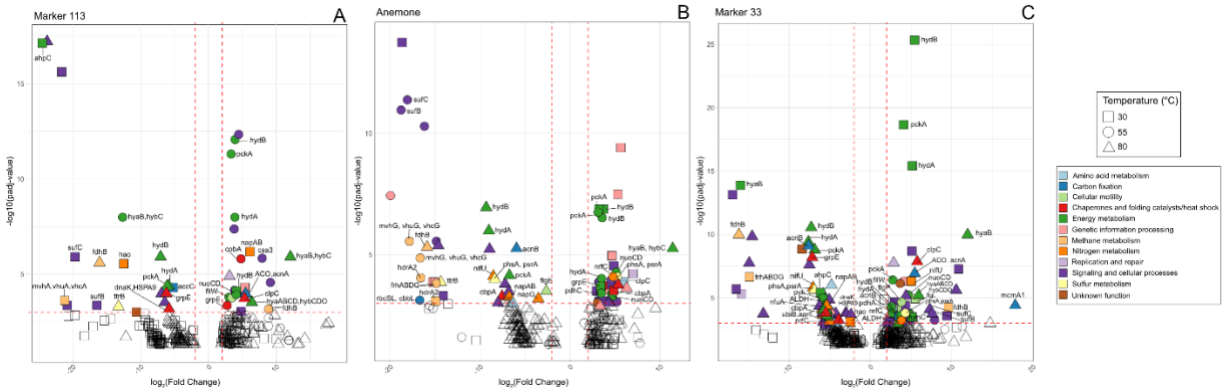

Figure 6. Volcano plots showing the $\log_2$FC (degree of differential expression) within each vent across experimental temperatures at **A.** Marker 113, **B.** Anemone, and **C.** Marker 33. Colored points correspond to genes that had a padj $< 10^{-3}$ and $\log_2$FC $> |2|$ (padj; p-value adjusted for multiple tests using the Bonferroni correction), but only genes involved in energy acquisition, central carbon metabolism, cellular motility, heat shock, Fe-S cluster assembly, and CRISPR/Cas system proteins are labeled with gene names.

Differential expression across vents by temperature

As noted, DE analysis was also carried out across vents by temperature. Across the three vents by each temperature, 240 unique transcripts were SDE 329 times and included transcripts of genes related to electron transport, carbon fixation, and carbon and nitrogen metabolism (Figure S7, Table S12). The greatest number of significantly differentially expressed transcripts were observed at 30°C. None were identified at 55°C, and 3 transcripts were SDE in 80°C experiments.

Differential expression across time within each vent

For DE analysis across time within each vent, 114 unique genes were SDE 161 times (Figure S8, Table S13), with most of them significantly upregulated in Marker 113 and Marker 33 in 2013. Annotated upregulated transcripts within sites with the greatest expression differences compared to the other sites across time were those related to methane metabolism (including *mcr* and *hdr*, among others), energy metabolism, and motility (Fig S8).

DISCUSSION

Diffuse hydrothermal vent fluids are a window into the subseafloor microbial community in young oceanic crust, representing one of the most productive regions of the deep sea. The microbial communities found in these fluids are taxonomically and functionally diverse and include a mix of seawater, seafloor, and subseafloor communities that inhabit temperatures from 2°C to near 100°C across a wide range of geochemical gradients, making it difficult to pinpoint the active microbes beneath the seafloor. In this study, we experimentally manipulated venting fluids to target subseafloor microbes under variable temperature and reducing conditions and used stable isotope labeling with inorganic carbon coupled to metatranscriptomic sequencing to focus on active autotrophic subseafloor microbes, their metabolic and growth strategies, and their distribution in the subseafloor.

Expanding upon decades of research at Axial Seamount, we analyzed 15 (21 total timepoints; Table 2) RNA-SIP experiments from 3 spatially separated vents in 2 consecutive years and hypothesized that the subseafloor autotrophic microbial population structure at each site would be distinct, with transcriptional metabolic profiles reflective of the geological and geochemical characteristics of each individual vent. While our results broadly corroborate this hypothesis, as well as building upon previous work at Axial Seamount that indicated microbial communities at individual vents host distinct microbial communities over multiple years (10, 12), by focusing on

411 only autotrophs at specific temperatures, we also found active cosmopolitan, subseafloor
412 autotrophs occupying particular thermal niches. In addition, while certain metabolisms and
413 associated lineages such as methanogenic archaea ("specialists") are restricted in distribution,
414 other metabolisms geared toward hydrogenotrophic sulfur and nitrate-based metabolisms and
415 microaerophily ("generalists") are widely distributed in many lineages across a wide temperature
416 range, highlighting metabolic flexibility and functional redundancy across diverse taxonomic
417 groups in this ecosystem. Competition for electron donors like hydrogen and electron acceptors
418 like oxygen was apparent in the data, as shifts in taxonomy and transcription highlighted the
419 conditions under which various microbial groups could dominate. The data suggest that while
420 chemical and physical characteristics at each vent control the energy available for microbial
421 growth—as is the case for methanogenesis and sulfide oxidation—some ubiquitous microbial
422 subseafloor lineages within the young oceanic crust at Axial Seamount have adapted to a broad
423 range of subseafloor chemistries and temperatures and are therefore not restricted in distribution.
424 We used multiple bioinformatic tools to examine this complex RNA-SIP
425 metatranscriptomic dataset, including transcript taxonomy to provide detailed microbial
426 community composition profiles (Fig 3) for each experiment, as well as experiment-derived MAG
427 read recruitment to determine specific population distributions (Fig 4). We also analyzed
428 taxonomy and activity of metabolism-specific genes (Fig 5), coupled with a functional-agnostic
429 approach with multiple differential gene expression analyses (Fig 6). Importantly, all RNA-SIP
430 experiments experienced a significant distillation of the taxa present in the unmanipulated fluid
431 metatranscriptomes (Fig 3). Of note is the reduction or disappearance of *Alpha*-, *Delta*-, and
432 *Gammaproteobacteria*, as well as *Actinobacteria*, groups that comprised up to half of the microbial
433 community in unmanipulated fluids and are common in plume and background seawater samples.

434 The RNA-SIP experiments were amended with hydrogen to re-create putative reducing
435 subseafloor conditions. Along with temperatures of incubation, this likely explains why these taxa
436 are not heavily represented in the RNA-SIP metatranscriptomes as they are either not adapted to
437 these subseafloor conditions or are heterotrophs. Here, we discuss some of the specific patterns of
438 taxonomic distribution coupled with the gene expression patterns and geochemical features across
439 the three vents to determine how the interplay of fluid chemistry, microbial competition, and
440 functional potential results in the presence or absence of microbial populations across vents and
441 temperatures.

442 The novel *in situ* oxygen sensor data enabled new insights into the important role of oxygen
443 for subseafloor microbial metabolism, even at high temperatures. Through linear regression
444 modeling of this data, we predicted oxygen was depleted to zero at temperatures of 33°C at Marker
445 113 and 52°C at Marker 33 but was predicted to be present at temperatures up to 100°C or more
446 at Anemone (Fig 1). The oxygen models align with the transcript data, as the presence of oxygen
447 at high temperatures at Anemone likely enabled the persistence of microaerophilic sulfide
448 oxidation in the 80°C experiments. This was indicated by the transcription of sulfide:quinone
449 oxidoreductase (*sqr*) for sulfide oxidation belonging to *Aquifex*, *Hydrogenivirga*, and *Phorcysia*.
450 However, at Marker 113 and Marker 33, this oxygen-dependent enzyme for autotrophy (32) was
451 not expressed above 55°C, consistent with the depletion of oxygen at lower temperatures at these
452 sites.

453 At all sites in all years, the geochemistry of the diffuse venting fluids indicated biological
454 utilization of hydrogen when compared with conservative mixing, with evidence for methane
455 production only at Marker 113 and Marker 33 (Fig 2). These geochemical indicators of biological
456 activity broadly map to the metabolism-focused analyses. Transcripts for methanogenesis were

457 restricted to Marker 113 and 33 (Fig 5). In addition, the top 30 expressed genes (TPM) at 55°C
458 and 80°C included those related to methanogenesis only at these two vents. This also corresponds
459 to the consistent activity of the singular, high quality *Methanothermococcus* MAG (Bin 335) at
460 Marker 113 and 33 (Fig 4). In contrast, at Anemone, methanogenesis-related transcripts were not
461 included in the top 30 expressed genes (Fig 5, Fig S6), and were overall significantly
462 downregulated at Anemone compared to other sites, likely due to the more oxic conditions
463 measured at this site (Fig 1, Fig 5).

464 Unlike the restricted distribution of transcripts for methanogenesis, all sites showed
465 biological utilization of hydrogen, and at Marker 113 and 33, also utilization of nitrate (Fig 2).
466 Transcripts for hydrogen and nitrate utilization were found widely across all conditions, and in
467 particular, the periplasmic nitrate reductase *napAB* and hydrogenase genes quinone-reactive Ni-
468 Fe hydrogenase (*hyd*), energy-converting hydrogenase (*ech*), and Ni-Fe hydrogenase (group 1)
469 (*hya*, *hyb;* Fig 5) were all upregulated in the differential expression analysis. The transcripts for
470 hydrogen oxidation coupled with nitrate reduction were associated with a diverse number of
471 genera, including *Sulfurimonas, Cetia, Hydrogenimonas,* and *Caminibacter* at 30°C; *Cetia,*
472 *Caminibacter, Nautilia, Hydrogenimonas* and those from phylum Aquificota at 55°C; and
473 *Thermovibrio* and *Desulfurobacterium* at 80°C (Fig 3). Chemical analysis of diffuse fluids showed
474 that there was higher H_2S concentrations in both 2013 and 2014 at Anemone than at the other two
475 vents (Table 1), correlating with high transcription of polysulfide/thiosulfate reduction genes *psr*
476 and *phs* (up to 14,000 TPM) in tandem with hydrogen oxidation (Fig 5). Taxa expressing both *psr*
477 and *phs,* along with Ni-Fe hydrogenase at Anemone, include *Cetia, Nautilia*, and
478 *Hydrogenimonas*; the latter is known to utilize oxygen as a terminal electron acceptor.

479 Within each year, there were also MAGs active in all vents in at least one time point:

480 *Hydrogenimonas* bin 102 (at 55°C in 2014), Nautiliaceae bin 340 (at 55°C in 2013 and 2014),
481 *Thermovibrio* bin 320 (at 80°C 2013 and 2014), and Desulfurobacteriaceae bin 324 (at 80°C in
482 2014). The recurrence of active MAGs across vents and temperatures indicates that some vents at
483 Axial Seamount host the same populations of microorganisms, agnostic of style of venting
484 (through basalt vs. sulfides) or geochemistry (Fig 4). Previous studies (e.g. 9-10, 16, 33 Olins)
485 determined that established subseafloor microbial communities are mostly restricted by local vent
486 fluid geochemistry and physical structuring of the site, but our results show this may not be true
487 for some lineages at the population level. Our data reveal that some cosmopolitan taxa are capable
488 of colonizing a wide range of environmental niches, functioning as ecosystem generalists. On the
489 other hand, lineages restricted in distribution, such as methanogens, may serve as an example of
490 ecosystem specialists.

491 Many of these cosmopolitan taxa that carry out hydrogenotrophic sulfur and nitrate
492 reduction are known to be efficient at oxidizing hydrogen. For example, a study done by Nishimura
493 *et al*. (2010) found that hydrogenases purified from the vent-endemic *Hydrogenimonas*
494 *thermophila* were phylogenetically related to pathogenic Campylobacterota, known to have high
495 hydrogen oxidation activity (34). Like *Hydrogenimonas,* another vent-endemic organism *Nautilia*
496 *profundicola* was found to have multiple operons for hydrogenases, including one H_2-sensing
497 (Group 2), two H_2-uptake (Group 1), and three H_2-evolving (Group 4) hydrogenases in their
498 genome. Consistent with the findings from cultured representatives of *Hydrogenimonas* and
499 *Nautilia* that highlight flexibility encoded in their genomes for hydrogen utilization (35), our MAG
500 analyses indicated that both taxa transcribed three of the four hydrogen marker genes at 55°C,
501 including quinone-reactive Ni-Fe hydrogenase (*hyd*), Ni-Fe hydrogenase (group 1) (*hya, hyb)*, and
502 energy converting hydrogenase (*ech*; Table S14).

503 Transcripts for hydrogenases were also detected at 80°C at both the community level and
504 in the ubiquitous Aquificota MAGs, supporting the prevalence and importance of hydrogen
505 oxidation in these taxa. Transcripts for three hydrogenase marker genes, Ni-Fe hydrogenase (group
506 1) (*hya*, *hyb*), energy-converting hydrogenase (*ech*), and sulfhydrogenase, are attributed to both
507 *Desulfurobacterium* and *Thermovibrio* (Fig 3, Fig 5, Table S9). Desulfurobacteriaceae bin 324
508 was found at all vents in 2014 and transcribed hydrogenase maturation protein *hypF* (Table S14).
509 *Thermovibrio* bin 374, found at all vents in 2013 and 2014, transcribed numerous hydrogenases,
510 including the F420-non-reducing hydrogenase, hydrogenase maturation protein *hypF,*
511 hydrogenase expression/formation proteins *hypED*, and multiple sulfhydrogenase subunits (Table
512 S14). The diversity and versatility of these hydrogenase genes likely enable these taxa to grow and
513 survive across vents with different chemistries, leading to the cosmopolitan nature of these
514 populations.

515 Hydrogen is also utilized by hydrogenotrophic methanogens at these vents, and
516 competition for hydrogen between methanogens and the cosmopolitan, hydrogenotrophic sulfur
517 and nitrate reducers of the Aquificota likely occurs in the subseafloor at temperatures >50 °C (36-
518 38). Methanogenic growth may be inhibited by growth of these other groups by bringing localized
519 H_2 concentrations to a partial pressure below which methanogenesis can occur (39-41). Cultivation
520 experiments showed that *Desulfurobacterium* strain HR11 has a lower H_2 requirement and lower
521 K_s than *Methanocaldococcus* (30 μM vs. 67 μM; 37, 42). In co-culture experiments with
522 *Methanothermococcus thermolithotrophicus* (T_{opt} 65°C), *Methanocaldococcus jannaschii* (T_{opt}
523 82°C), and *Desulfurobacterium thermolithotrophum* (T_{opt} 72°C), Kubik and Holden (2024) found
524 that *D. thermolithotrophum* outcompeted both methanogens at high and low hydrogen
525 concentrations when grown at a 1:1 ratio of initial inoculum (36). However, when *M.*

526 *thermolithotrophicus* was grown at a ratio of 10:1 with *D. thermolithotrophum*, the methanogen
527 outcompeted the bacterium, suggesting the conditions under which methanogens can successfully
528 establish first and grow in larger numbers, as observed in the 55°C experiments at Markers 113
529 and 33 where methanogens were in higher abundance.

530 An additional factor that can influence the distribution and metabolic strategies of
531 hydrogen-utilizing microbes are physical characteristics of the hydrothermal vents. Building off a
532 reactive transport model developed to examine thermophilic vs hyperthermophilic methanogen
533 growth at Axial vents (28), Kubik and Holden expanded the model with additional
534 hydrogenotrophic autotrophs and determined that when the residence time of subseafloor fluids
535 was long, methanogens dominated, but when fluids had shorter residence times, Aquificota
536 dominated. Lower temperatures combined with longer residence times also favored thermophilic
537 methanogenic growth (36). Taken together, our results support these cultivation and modeling
538 studies and show that in the natural world, methanogens require more specific physicochemical
539 conditions for successful growth, thus limiting their distribution, whereas diverse Aquificota and
540 Campylobacterota are more metabolically flexible and less dependent on geochemistry
541 constrained by fluid residence times, enabling a more cosmopolitan distribution. Anemone's close
542 (<1 m) proximity to a high temperature (~300°C) end-member may create short subseafloor fluid
543 residence times; in contrast, Marker 113 and Marker 33 are located farther (~750 m) from a high-
544 temperature venting source, supporting longer fluid residence times, and thus methanogens. Our
545 coupled geochemical and meta-omics results suggest that the distribution of some subseafloor
546 microbes may be determined by both a microbe's efficiency and genetic regulation of hydrogen
547 utilization as well as the interspecies relationships, chemistry, residence time, and temperature of
548 the subseafloor venting fluids.

549 Microbial community composition shifted with temperature and vent location.
550 Campylobacterota dominated all RNA-SIP metatranscriptomes until 80°C, when methanogens and
551 members of the Aquificota became the key carbon-fixing phyla. At 30°C, ORF-based transcript
552 analysis attributed a substantial proportion of transcripts to *Sulfurimonas* at Marker 113 and
553 *Hydrogenimonas* at Marker 33 (Fig S9). Fluid chemistry may explain why these genera are the
554 dominant autotrophs in these low-temperature conditions at each respective vent. Diffuse fluids in
555 both Marker 113 and Marker 33 had comparable H_2 concentrations across the years, though 10x
556 lower than those in Anemone, but the oxygen-temperature trends observed in water samples
557 predicted zero-oxygen (anoxia) at temperatures above 55°C (Fig 1). In our study, *Sulfurimonas*
558 was especially active and abundant in Marker 113 at 30°C. The O_2 concentration measured at
559 Marker 113 was consistently the lowest of all three vents each year (7.0 µM in 2013, 9.9 µM in
560 2014, Fig 1, Table 1). While fluid residence times and flow rate impact oxygenation, Marker 113's
561 comparatively low oxygen concentrations may be in part due to *Sulfurimonas* O_2 consumption. In
562 the 30°C expression profiles of Marker 113 and Anemone, the only terminal electron acceptor
563 *Sulfurimonas* transcribed was cytochrome c oxidase, *cbb*$_3$-type (*ccoNOPQ*), suggestive of a
564 metabolism of oxygen reduction and hydrogen oxidation (Fig 5, Fig S9, Table S9). Given the
565 absence of *Hydrogenimonas* metabolic transcripts and the overall dominance of *Sulfurimonas* in
566 transcriptional profiles of Marker 113 at 30°C, the depleted activity of microaerophilic
567 *Hydrogenimonas* may reflect more stringent conditions (e.g. less H_2 and less O_2), and/or
568 competition with *Sulfurimonas* for oxygen as an electron acceptor. On the other hand, the
569 metabolic versatility and higher growth optimum temperature of *Hydrogenimonas* may provide
570 for its continued activity level at higher temperatures, where it can utilize alternative electron

571 acceptors such as nitrate, nitrite, and sulfur (34). In our experiments, *Hydrogenimonas* was more
572 abundant at all sites at 55°C than at 30°C.

573 At Marker 33, *Sulfurimonas* and *Hydrogenimonas* were almost in equal proportion in 30°C
574 transcriptional profiles for both years. These taxa transcribed genes for multiple electron acceptors,
575 including oxygen (*cco)*, nitrate (*napAB*), nitrite (*nir, nar*, *nxr*), and sulfur (*sox*, *sqr*; Fig S9).
576 *Sulfurimonas* are capable of oxidizing S^0 and H_2, reducing O_2 and NO_3^-, using various carbon
577 sources, and thriving in microaerophilic and anaerobic conditions, typically below 40°C (Table
578 S9; 14, 43-45). *Hydrogenimonas* bins 102 and 104 expressed a high percentage of their coding
579 genomes in 30°C fluids of Marker 33, and transcripts assigned to *Hydrogenimonas* had low
580 abundance in the other vents at 30°C (Fig 4). The presence of oxygen up to 52°C, closer to the
581 growth optimum of *Hydrogenimonas,* may mean that both *Sulfurimonas* and *Hydrogenimonas* can
582 use oxygen at higher temperatures at this site (Fig 1, Table S2). On the other hand, these sustained
583 oxygen concentrations up to 52°C may also hinder establishment of taxa with similar metabolisms,
584 higher optimum growth temperature, but lower oxygen tolerance than *Hydrogenimonas* (e.g.
585 *Caminibacter, Cetia, Lebetimonas*, and *Nautilia*).

586 *Conclusions*

587 This study identified subseafloor microbial primary producers at 3 spatially separated vents
588 over 2 years at Axial Seamount and enabled a granular view of the autotrophic microbes at the
589 base of the deep-sea hydrothermal vent ecosystem. The active autotrophs vary between vents but
590 less so over time, demonstrating that vent geology, fluid chemistry, and flow path shape the
591 geochemical environments and active metabolisms observed. This dynamic interplay between
592 microbial metabolism and vent fluid chemistry not only influences the community structure but
593 also determines which groups dominate under varying environmental conditions. Hydrogen and

594 oxygen availability and utilization is a key control for the establishment of autotrophs, with
595 competition between autotrophic sulfur-reducing taxa and methanogens for H_2 evident. These
596 interactions underscore the complex ecological networks at hydrothermal vents, where microbial
597 communities not only adapt to but also actively shape their environment through metabolic
598 exchanges and niche differentiation. Spanning a range of geochemical regimes, these findings
599 illuminate the intricate microbiological networks at deep-sea hydrothermal vent systems and
600 highlight the active functions of key carbon-fixing taxa and their interactions within microbial
601 communities in the circulating subseafloor crustal fluids.

602 **MATERIALS AND METHODS**

603 *Sample collection*

604 Axial Seamount samples were collected using ROVs ROPOS and JASON aboard the *R/V*
605 *Falkor* and *R/V Thompson* in September 2013 and *R/V Brown* in August 2014 (8, 10).
606 Hydrothermal plume water from 42 m above Anemone (N 45.9335667, W 130.013667) and
607 ambient seawater at 1500 m depth (N 46.27389, W 129.79548) were also collected using a Seabird
608 SBE911 CTD equipped with 10 L Niskin bottles in 2015 aboard the *R/V Thompson*, 5-months
609 post-eruption at Axial Seamount. Water was transferred from Niskin bottles into cubitainers, and
610 3 L was filtered through 0.22 µm Sterivex filters (Millipore, Billerica, MA, USA) for later
611 metagenomic sequencing.

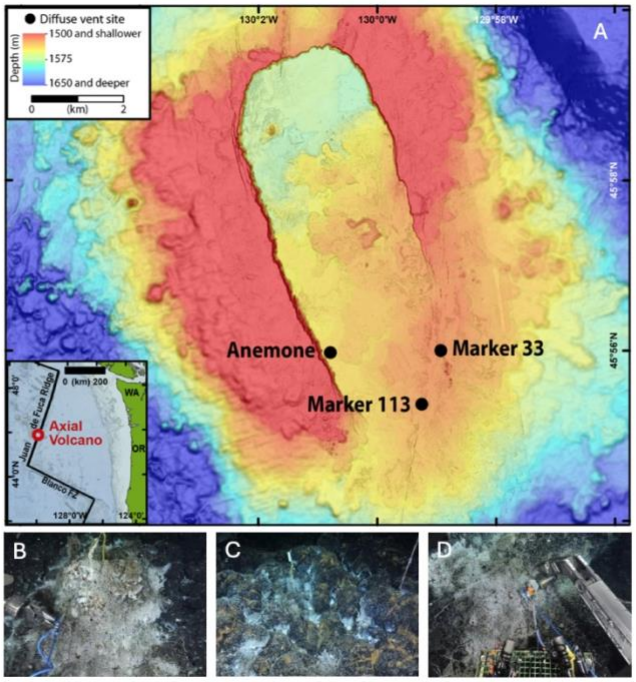

Figure S1. Map of Axial Seamount a. showing locations of the three diffuse vents sampled, including Marker 113, Anemone, and Marker 33. Map from Fortunato *et al*., 2018 (10). Images from ROV Jason (WHOI).

The Hydrothermal Fluid and Particle Sampler (HFPS; 27) and Large Volume Water Sampler (LVWS; 46) were used to collect fluids at ~2 cm above the seafloor. The coordinates for each vent are Marker 113: N 45.9227, W 129.9882; Anemone: N 45.9332, W 130.0137; Marker 33: N 45.9332, W 129.9822. Temperature was monitored while drawing fluids using an integrated temperature sensor that was present on both samplers. For sampling with the HFPS and LVWS, a 4 L capacity acid-washed Tedlar bag or a 5 L acid-washed plastic carboy, respectively, was used to collect fluids for RNA-SIP experiments as described in (8). DNA and RNA from diffuse fluids for metagenomic (2013-2015) and metatranscriptomic (2013 and 2014) sequencing were concurrently collected using the HFPS at a rate of 100–150 mL min^{-1} through a 0.22 µm, 47 mm GWSP filter (Millipore) for a total volume of 3 L. All filters were preserved *in situ* with RNALater

(Ambion, Grand Island, NY, USA) as described in Fortunato *et al.* (2018) (10). RNA-SIP experiments are reported here only from 2013 and 2014, since there were too few samples from 2015 to include in the analysis, though the unmanipulated diffuse fluid metagenomes were included in assemblies to provide more phylogenetic and functional coverage representative of the Axial diffuse fluid microbial community.

Hydrothermal fluid samples were collected with the Hydrothermal Fluid and Particle Sampler (HFPS) following procedures described in (27). Vent fluid samples were analyzed on board for pH, total H_2S, and dissolved methane and hydrogen. Magnesium and nitrate were analyzed on shore. With the exception of oxygen data, these chemical data were previously reported in (10) and used for methanogen modeling in (28). For this study, HFPS included an oxygen optode (SeaBird SBE 63) capable of measuring oxygen concentration in fluids up to a maximum of 40°C. Temperature was monitored at the sample intake, near the sensor block, and inside the oxygen sensor housing. Oxygen measurements were made just before or after collecting fluid samples, with the intake in the same position to replicate collected water samples. Water was pulled from the titanium/Teflon sampling manifold through the sensor, with some cooling taking place along the flow path. The SBE63 optode does not require constant flow rate, does not consume oxygen, and can make measurements when flow is stopped. The SBE63 sends 1 Hz serial data, which is received by the HFPS on-board computer. Oxygen concentration is calculated using the temperature measured in the sensor housing, the ambient pressure and salinity (derived from ROV sensors and input manually to the software), and the factory calibration. The factory calibration covers a temperature range from 2°C to 30°C. All of the measurements for this study had temperatures at the sensor within the calibration range. Over the 2013-2015 period of this study, the average oxygen concentration of near-bottom seawater within the caldera, where all diffuse

650 vents for this study are located, was 31 µmol/kg (+/- 2µmol/kg, n=24). Oxygen increases
651 significantly with increasing depth at Axial Seamount, where the summit is below the oxygen
652 minimum.

653 *RNA-SIP experimental procedures*

654 For LVWS samples in 2013, fluid from carboys was pumped using a peristaltic pump into
655 evacuated 1 L Pyrex bottles with air-tight butyl stoppers to a volume of 1060 mL. For all other
656 samples in 2013 and 2014, fluid was pumped using a peristaltic pump from the sampling bags or
657 carboys into evacuated 500 mL Pyrex bottles with air-tight butyl stoppers to a volume of 530 mL.
658 During filling, steps were taken to minimize introduction of oxygen and outgassing of fluid. Prior
659 to filling, ^{13}C-labeled sodium bicarbonate (Cambridge Isotope Laboratories, Tewksbury, MA,
660 USA) for the experimental condition or ^{12}C-labeled sodium bicarbonate (Sigma, St. Louis, MO,
661 USA) for the control condition was added to each bottle to a final concentration of 10 mM over
662 background. After filling, the pH of each bottle was adjusted to vent fluid pH (<6.5), using 1–2.5
663 mL of 10% HCl. The headspace was filled with pure H_2 gas using a syringe in the quantity 20 mL
664 (900 µmol) for each 500 mL bottle and 60 mL (2700 µmol) for the1 L bottles. ^{12}C- and ^{13}C-
665 bicarbonate amended bottles were each incubated at 30, 55, and 80°C for various times as shown
666 in Table 2 in the main text. After incubation, the fluid in each bottle was filtered through 0.22 µm
667 Sterivex filters (Millipore), preserved in RNALater (Ambion), and frozen at −80°C.

668 RNA from SIP experiments was extracted according to (8) and detailed in the Supplementary
669 Information (SI). Following RNA extraction and quantification, each RNA-SIP experiment
670 required isopycnic centrifugation to separate the heavy RNA (labeled with ^{13}C—the active
671 autotrophs) from the light RNA (members of the community that did not take up the ^{13}C label,
672 representing the less active members of that community) as described in (8) and the SI.

673 Four metatranscriptomic libraries were constructed for each RNA-SIP experiment: two from
674 the ^{12}C-control (^{12}C-light and ^{12}C-heavy) and two from the ^{13}C-experiment, (^{13}C-light and ^{13}C-
675 heavy) as described in (8) except for four samples: the second timepoints in 2014 of Marker 113
676 at 55°C and Marker 33 at 30°C and 80°C and the only timepoint at Anemone at 80°C. The ^{12}C-
677 control incubation peak(s) of highest RNA concentration were used to construct the ^{12}C-light
678 library, which represents the natural community. Similarly, the ^{13}C-experiment incubation peak(s)
679 of highest RNA concentration were used to construct the ^{13}C-heavy library, which represents the
680 labeled, active autotrophic community. The other two libraries from each temperature, ^{12}C-heavy
681 and ^{13}C-light were constructed to act as additional controls but were not taken through full
682 bioinformatic processing. In some cases (denoted in Figs S3-5), two RNA fractions were combined
683 for library construction.

684 *Metagenomic bioinformatic analyses*

685 There were 11 metagenome samples processed, including metagenomes from all three vent
686 sites in 2015 (Table S4; 10). These samples were included to provide a comprehensive functional
687 repertoire in diffuse fluid communities at Axial Seamount (10). A pipeline with code used in
688 metagenomic processing can be found here: https://github.com/corporeal-snow-albatross-
689 5/Axial_Metagenomics. Samples were first trimmed of Illumina adapter sequences using
690 Trimmomatic (v0.32; 47), quality controlled using FastQC (v0.11.9; 48), and quality results were
691 aggregated across samples into a single report using MultiQC (v1.12; 49). These initial trimming
692 and quality control steps were done using the qc-trim Snakemake pipeline designed by Dr. Sarah
693 Hu (https://github.com/shu251/qc-trim). The separate forward reads and separate reverse reads
694 were concatenated using the cat command in Unix, and then concatenated forward and reverse
695 read files were combined using the fq2fa (v1.1.3) function within the IDBA_UD assembler (50;

696 https://github.com/loneknightpy/idba). Each of the metagenomes were assembled using
697 IDBA_UD (v1.1.3), using a max kmer size of 120 (50; https://github.com/loneknightpy/idba).
698 Contig and scaffold quality was evaluated using MetaQUAST (v5.0.2; 51), and the best assembly
699 given steps of 20 from kmer lengths of 20-120 was chosen for further analysis. Each metagenome
700 was submitted to the DOE Joint Genome Institute's Integrated Microbial Genome Expert Review
701 (IMG/ER) for annotation. IMG/ER JGI GOLD Analysis Project ID numbers can be found in
702 Supplementary Table 1. Open reading frame (ORF) information from the IMG/ER annotation was
703 extracted using a python script (gff2seqfeatures.py; courtesy of Dr. Connor Scannerton) to create
704 .ffn files from. gff (containing contig and locus identity, start and stop sites of ORFs, and strand
705 information) and .fna files (containing the nucleotide sequence of each ORF). All metagenome
706 .ffn files were then concatenated to make one long, annotated assembly using the cat command in
707 Unix.

708 The ORFs predicted in each metatranscriptomic (mRNA) file were mapped back to the
709 concatenated metagenomic assembly, which was first indexed using the kallisto index function
710 within the pseudoaligner Kallisto prior to mapping (v.0.46.0; 52). Post-mapping, the Kegg
711 Ontology (KO) ID's and the taxonomy of each predicted ORF in the metagenomes were retrieved
712 from IMG/ER. Cutoffs on the minimum requirements of an e-score of 10^{-10}, 30% amino acid
713 identity, and alignment length of 40 amino acids were imposed, as used in (10). The filtered KO
714 tables of each metagenome were concatenated with each other, and the same was done for the
715 taxonomy tables. The concatenated KO and taxonomy tables were then combined with each other
716 using an inner_join in the R dplyr package, based on target_id (predicted ORF).

717

718

719 *Metagenome Assembled Genome (MAG) generation and analysis*

720 In addition to an annotated, concatenated assembly, a co-assembly using the quality-
721 filtered and trimmed reads from 11 metagenomic samples was also constructed using MEGAHIT
722 (v1.2.9; 53) with parameters --min-contig-len = 200, --presets = "meta-sensitive". Assembly
723 statistics were checked using MetaQUAST (v5.0.2; 51). The resulting assembly had 2,318,625
724 contigs that were at least 500 bp in length; of those contigs, the N50 = 721bp and maximum length
725 = 280,659bp. The co-assembled metagenome (hereafter referred to as the "co-assembly") was
726 annotated through the DOE Joint Genome Institute's Integrated Microbial Genome Expert Review
727 (IMG/ER) pipeline. IMG/ER JGI GOLD Analysis Project ID numbers can be found in
728 Supplementary Table 1. The resulting gene calls, GFF annotation file, and phylodist taxonomy of
729 contigs, were used as the reference material for the metagenome assembled genomes (MAGs),
730 differential gene expression analyses, taxonomy assessments, and overviews of functional
731 potential vs expression. Kegg Ontology (KO) ID's and the taxonomy of each predicted ORF in the
732 co-assembly were retrieved from IMG/ER. Cutoffs on the minimum requirements of an e-score of
733 10^{-10}, 30% amino acid identity, and alignment length of 40 amino acids were imposed, as used in
734 (10).

735 MetaBAT2 (v2.15; 54) was used to generate metagenome-assembled genomes (MAGs).
736 The co-assembly was first indexed using the bwa index within BWA mem (v7.17; 55) and then
737 metagenomes were mapped to the indexed file. The resulting output was processed through
738 Samtools (v1.13; 56). The .sam file generated from mapping was converted to a .bam file using the
739 samtools view function and resulting .bam files were sorted using samtools sort. Prior to binning,
740 depth (also called coverage) files were created for each metagenome and binned with minimum
741 contig length of 1500 using MetaBAT2. DAS Tool was then used to resolve redundancy between

742 bins and provide an optimized bin set (v1.1.7, 57). Bins were taxonomically classified using
743 GTDB-tk (v2.1.1; 58).

744 Genomic binning from all of the diffuse fluid metagenomes resulted in 391 MAGs, and
745 after removing redundant bins using DAS Tool (v1.1.7; 57), 120 bins remained with 45 having <
746 10% contamination and being >70% complete (Table S6). The MAGs were further filtered to
747 remove heterotrophs and samples solely sourced from the plume, background, or 2015
748 metagenomes, resulting in 25 bins remaining. The final 11 MAGs were selected based on having
749 >4% of their coding genome expressed (length of expressed genes(bp)/genome length (bp); Fig 4
750 in the main text, Table S7) in any individual RNA-SIP ^{13}C-heavy fraction.

751 *Metatranscriptomic bioinformatic analyses*

752 In total, there were 96 metatranscriptome samples processed total: 6 diffuse fluid
753 metatranscriptomes from unmanipulated fluids at each vent in 2013 and 2014 and 90 RNA-SIP
754 metatranscriptomes (Tables S3, S4). Metatranscriptomic sequences were trimmed and quality
755 checked with the same methods and software parameters as the metagenomic sequences. The
756 separate forward reads and separate reverse reads were concatenated using the cat command in
757 Unix, and then concatenated forward and reverse read files were combined using Fast Length
758 Adjustment of Short reads (FLASH; v.1.2.11; 59), which is a program used to combine fastq files.
759 The only parameter set was for read length, which was 110bp. Although metatranscriptome
760 libraries were constructed with selective amplification for mRNA (not rRNA), the SIP
761 metatranscriptomes were not. To separate the rRNA for preliminary taxonomic analyses from the
762 mRNA for downstream processing, SortMeRNA (v4.2.0; 60) was used (Table S5). The SILVA
763 v.132 bacterial and archaeal 16S (id85), 23S (id98), and 5S (id98) databases were used as the
764 reference databases to map the rRNA. The rest of the parameters were: --fastx for a fastq output

765 format, --other for mRNA reads that did not map to the databases, --out2, and --pairedout for non-
766 aligned reads. The percentage of reads mapping to rRNA from SortMeRNA can be found in Table
767 S4.

768 Fastq reads from SortMeRNA rRNA output were converted to fasta format using the fq2fa
769 (v.1.1.3) function within IDBA_UD assembler (50; https://github.com/loneknightpy/idba). rRNA
770 taxonomy was classified using mothur classify.seqs function and the SILVA (v.132) 16S rRNA
771 reference database (61). The 5S rRNA database used as one of the reference databases for rRNA
772 mapping in SortMeRNA also contains eukaryotes. As such, the eukaryote hits were removed
773 before further processing. Taxonomy count tables were generated using R, and bar plotting for
774 rRNA was done via ggplot2 within tidyverse in R. Resulting plots were only used to compare to
775 ORF transcript taxonomy and are not included in this paper.

776 Fastq mRNA reads were mapped to the indexed concatenated metagenomic assembly using
777 the kallisto quant function within Kallisto (v0.46.0; 52), which also normalized all ORFs that
778 mapped, providing transcripts per million (tpm) values for each ORF. Sample names were attached
779 to kallisto output files, then all files were concatenated and tpm values of 0 were removed. This
780 table was then attached to the KO and taxonomy table made from the IMG/ER output using an
781 inner_join in the R dplyr package, based on target_id (predicted ORF). 784,486 total ORFs from
782 all samples joined out of 4,027,381 total, which means that 80.521% of ORFs from the
783 concatenated metagenome were unmatched in KO and taxonomy in the metatranscriptomes and
784 SIP metatranscriptomes. There were no eukaryote hits in the ORFs that had a match with both KO
785 and taxonomy. There were only 11 virus hits in these samples of 784,486 total ORFs that did have
786 matching KO's and taxonomy. Because few viruses and no eukaryotes were found, they were

787 removed for further processing and to enable comparability between the rRNA and ORF taxonomy.
788 All figures and statistical analyses were completed in R.

789 *Differential expression analysis*

790 Metatranscriptomic (mRNA) samples from the ^{13}C-heavy fractions of Marker 113,
791 Anemone, and Marker 33 incubations at 30, 55, and 80°C from 2013 and 2014 were pseudoaligned
792 to the indexed co-assembly using kallisto (parameters: --single -l 151 -s 41) (v0.46.0; 52). The
793 kallisto outputs of metatranscriptome pseudocounts were tabulated with the R package tximport
794 (v1.26.1; 62) using an annotation database of consolidated gene families. Due to the diversity in
795 metagenomes, the co-assembly annotation contained multiple targets for gene products. To reduce
796 complexity in functional expression analyses, genes observed in the co-assembly were
797 consolidated into protein families using IMG's highest confidence annotation such as KEGG,
798 COG, pfam, and TIGRFAM. ORFs annotated with only "hypothetical protein" were discarded.
799 The annotation database consolidated 2,428,812 unique genes into 14,942 gene families observed
800 in the co-assembly. When referring to genes and proteins in our evaluations of differential
801 functional expression, we are using the consolidated gene families.

802 Differential expression analyses were conducted in R with DESeq2 (v1.38.3; 63). To
803 reduce stochasticity and improve assessment of significant genes, we tailored baseline (control)
804 gene expression for each of the comparisons: within-vent by temperature (1030 significantly
805 differentially expressed (SDE) transcripts; Table S11), across vents by temperature (329 SDE
806 transcripts; Table S12), and across time within each vent (161 SDE transcripts; Table S13). For
807 temperature comparisons within each vent (i.e. all Anemone experiments at 30, 55, and 80°C
808 compared to one another), the baseline expression for genes was the normalized expressions of all
809 metatranscriptomic samples (N=21; Table S2). For across vent comparisons at a single

810 temperature (i.e. All 30°C experiments, Anemone to Marker 113 to Marker 33), as well as
811 comparisons across time within each vent (i.e. 2013 Marker 113 80°C incubation compared to
812 2014 Marker 113 80°C incubation), gene baseline expressions were calculated at each incubation
813 temperature: 6 samples at 30°C; 8 samples at 55°C; and 7 samples at 80°C. Volcano plots show
814 genes with p-values adjusted for multiple test correction (Bonferroni) padj < 0.001 and $\log_2$ fold-
815 change > |2|; only genes involved in energy acquisition, central carbon metabolism, cellular
816 motility, heat shock, and some signaling and cellular processes are labeled with their gene names
817 on the figures (Fig 6, Figs S7, S8).

818 **DATA AVAILABILITY**

819 All raw metagenomic and metatranscriptomic read data are publicly available through the
820 Sequence Read Archive (SRA). Metagenomic assemblies are publicly available through JGI
821 GOLD. All accession numbers are located in Table S4.

822 **ACKNOWLEDGEMENTS**

823 This work was funded by the Gordon and Betty Moore Foundation Grant GBMF3297; the
824 NSF Center for Dark Energy Biosphere Investigations (C-DEBI) (OCE-0939564), contribution
825 number TBD, NOAA/PMEL, contribution number TBD; the Joint Institute for the Study of the
826 Atmosphere and Ocean (JISAO) under NOAA Cooperative Agreement NA15OAR4320063,
827 contribution number TBD; and the National Aeronautics and Space Administration (NASA) grant
828 number 80NSSC19K1427.

829 The NOAA/PMEL supported this work with ship time in 2014 and through funding to the
830 Earth Ocean Interactions group. The 2013 data collected in this study includes work supported by
831 the Schmidt Ocean Institute during cruise FK010–2013 aboard R/V Falkor. The NOAA/PMEL
832 (through funding to the Earth Ocean Interactions group) and GBMF supported field work in 2014

with ship and vehicle time aboard the R/V Brown (RB2014-03). We thank the captains and crews of the *R/V Falkor, R/V Thompson* and *R/V Brown* as well as the outstanding ROV teams of the vehicles *ROPOS*, *SuBastian*, and *JASON*.

Sarah Hu and Margrethe Serres provided guidance on the analysis and code used to process this dataset, while the Keck Facility at the Josephine Bay Paul Center at the Marine Biological Laboratory provided support for sequencing. Kevin Roe, Noah Lawrence-Slavas, Susan Merle, Andra Bobbit, and William Chadwick provided support at sea.

SUPPLEMENTARY INFORMATION

Tables:

1. **Table S1**: Chemistry
2. **Table S2**: Oxygen data
3. **Table S3:** Metatranscriptome and RNA-SIP Metatranscriptome Samples
4. **Table S4:** Sample accession numbers
5. **Table S5**: SortMeRNA Results: percent rRNA in the metatranscriptome samples
6. **Table S6:** MAG statistics for high completeness, low contamination bins
7. **Table S7:** Input data to the MAGs
8. **Table S8:** Input data to the bubble plots.
9. **Table S9:** Functions represented in the bubble plot and the taxa doing them
10. **Table S10**: Table with number of SDE genes by condition
11. **Table S11:** within-vents by temperature, DE analysis
12. **Table S12:** across-vents by temperature, DE analysis
13. **Table S13**: within-vents by time, DE analysis
14. **Table S14:** hydrogenases in the community functional analysis and bins

Figures:

1. **Figure S1**: Map of Axial
2. **Figure S2**: Cl^- vs Mg
3. **Figure S3**: qPCR at 30°C
4. **Figure S4:** qPCR at 55°C

861 5. **Figure S5:** qPCR at 80°C
862 6. **Figure S6:** Top 30 TPM at each temperature
863 7. **Figure S7:** Volcano plot of differential expression by temperature across vents
864 8. **Figure S8:** Volcano plot of differential expression between 2013-2014 at eacg vent
865 9. **Figure S9:** *Sulfurimonas* vs *Hydrogenimonas* transcribed electron acceptors

866 **SUPPLEMENTARY METHODS**

867 **RNA Extraction from Sterivex filter**

868 RNA from SIP experiments was extracted according to (8) by first cutting the Sterivex
869 filter into pieces with a sterile razor blade then following the protocol in the mirVana miRNA
870 isolation kit (Ambion). Biological material was removed from the filter pieces with a bead-beating
871 step using RNA PowerSoil beads (MoBio, Carlsbad, CA, USA), followed by an extraction with
872 acid phenol:chloroform. A total volume of 100 µL RNA was extracted and any remaining DNA
873 was removed using the Turbo-DNase kit (Ambion).

874 **Isopycnic centrifugation, fractionation and qRT-PCR**

875 Following RNA extraction and quantification, each RNA-SIP experiment required
876 isopycnic centrifugation to separate the heavy RNA (labeled with ^{13}C — the active autotrophs)
877 from the light RNA (members of the community that did not take up the ^{13}C label, representing
878 the less active members of that community) as described in (8). To prepare the gradient solution
879 for each sample, 5.1 mL of CsTFA (~2 g mL-1; GE Healthcare Life Sciences, Piscataway, NJ,
880 USA), 185 µL formamide, and a mixture of 500-750 ng RNA and gradient buffer solution (0.1 M
881 Tris-HCl, 0.1 M KCl, 0.1 mM EDTA) up to 1 mL were first mixed in a 15 mL falcon tube prior
882 to centrifugation (25). Once mixed, the refractive index was measured for each sample to ensure a
883 median RI of 1.3729 +/- 0.0002, equating to a density of ~ 1.80 g mL-1. Samples were then loaded
884 into 4.9 mL OptiSeal tubes (Beckman Coulter, Brea, CA, USA), weighed to ensure proper balance,
885 placed into a VTi 65.2 vertical rotor (Beckman Coulter), and spun at 37,000 r.p.m. at 20 °C for 64

886 hr using an Optima L-80 XP ultracentrifuge (Beckman Coulter). Each gradient was fractionated
887 into 12 tubes of approximately 410 µL each. The refractive index of each fraction was measured
888 to determine density as described by Lueders, 2010 (25; Equation 1). RNA was precipitated with
889 ice-cold isopropanol and the pellet was washed with ice-cold 70% ethanol as also as described in
890 (250. Following centrifugation, the RNA concentration of each fraction was determined using the
891 RiboGreen quantification kit (Invitrogen) and a Gemini XPS plate reader (Molecular Devices,
892 Sunnyvale, CA, USA). The RNA concentration was used as the guide for selecting which fractions
893 to sequence. Quantitative reverse transcription polymerase chain reaction (qRT-PCR) was used
894 to determine the quantity (copy number) of the 16S rRNA gene within each fraction using the
895 KAPA Biosystems SYBR FAST One Step RT-qPCR (ABI Prism) and the Universal 16S rRNA
896 primers, Pro341F and Pro805R primers (64). E. coli ribosomal RNA was used to construct a
897 standard curve. Results were used to determine the ratio of maximum quantity of 16S rRNA within
898 each set of fractions, that is the ratio of 16S rRNA in each fraction to the maximum copy number
899 across all fractions (25; Supplementary Figures 2-4).

900 **Equation 1.** Lueders equation for fraction density (CsTFA + Gradient Buffer + Formamide)

901 $y = -1893.9820x2+5230.8018x-3609.6804$

902 **Metatranscriptomic Library Construction**

903 Library construction for RNA-SIP fractions was carried out as described in Fortunato and
904 Huber and in the SI. Double stranded cDNA was constructed using SuperScript III First-strand
905 synthesis system (Invitrogen, Grand Island, NY, USA) and mRNA second strand synthesis module
906 (NEB, Ipswich, MA, USA). The synthesized double stranded cDNA was sheared to a fragment
907 size of 175 bp using a Covaris S-series sonicator (Woburn, MA, USA). SIP metatranscriptomic
908 library construction was completed using the Ovation Ultralow Library Complete Prokaryotic

909 RNA-Seq DR multiplex system (Nugen, San Carlos, CA, USA) following manufacturer
910 instructions, amplified using 15 cycles. Ribosomal RNA was not removed before construction of
911 libraries. Sequencing was performed on an Illumina HiSeq 1000 at the W.M. Keck sequencing
912 facility at the Marine Biological Laboratory in Woods Hole, MA. All libraries were paired-end,
913 with a 30 bp overlap, resulting in an average merged read length of 110 bp.

914 The 47 mm flat filters that were collected and preserved in situ for metagenomic and
915 metatranscriptomic sequencing were processed according to (10). The filters were first cut in half
916 with a sterile razor, half used for DNA extraction for metagenomic sequencing and half used for
917 RNA extraction for metatranscriptome sequencing. For DNA extraction, the DNA filter was rinsed
918 with sterile PBS to remove the salts from the RNAlater and was then extracted using a phenol-
919 chloroform method adapted from (65) and (66). DNA was then sheared to a fragment size of 175
920 bp (2013 and 2014) or 275 bp (Anemone, Marker 33, Marker 113 metagenomes from 2015, plume,
921 and background seawater) using a Covaris S-series sonicator. Metagenomic library construction
922 was completed using the Ovation Ultralow Library DR multiplex system (Nugen) following
923 manufacturer instructions.

924 **Metagenomic and Metatranscriptomic Sequencing**

925 Metagenomic and metatranscriptomic sequencing was done on an Illumina HiSeq 1000 in
926 2013 and 2014 and an Illuma NextSeq 500 in 2015. All libraries were paired-end, with a 30 bp
927 overlap, resulting in an average merged read length of 110 bp for libraries from 2013 and 2014
928 and 151 bp for libraries from 2015. Metagenomic and metatranscriptomic sequencing was carried
929 out at the W.M. Keck sequencing facility at the Marine Biological Laboratory in Woods Hole,
930 Massachusetts.

931 **REFERENCES**

932 1. Dick GJ. 2019. The microbiomes of deep-sea hydrothermal vents: distributed globally, shaped
933 locally. *Nat Rev Microbiol* 17:271–283.
934 2. Jannasch HW, Mottl MJ. 1985. Geomicrobiology of deep-sea hydrothermal vents. *Science*
935 229:717–725.
936 3. Summit M, Baross JA. 2001. A novel microbial habitat in the mid-ocean ridge subseafloor.
937 *Proc Natl Acad Sci* 98:2158–2163.
938 4. Reysenbach A-L, Shock E. 2002. Merging genomes with geochemistry in hydrothermal
939 ecosystems. *Science* 296:1077–1082.
940 5. McCollom TM. 2005. Energetic constraints on subsurface biomass production within the
941 igneous ocean crust. *Geochimica et Cosmochimica Acta* 69:A200.
942 6. Huber JA, Holden JF. 2008. Modeling the impact of diffuse vent microorganisms along mid-
943 ocean ridges and flanks. *In* Magma to Microbe: Modeling Hydrothermal Processes at Ocean
944 Spreading centers Jan 1;178:215-31.
945 7. Amend JP, McCollom TM, Hentscher M, Bach W. 2011. Catabolic and anabolic energy for
946 chemolithoautotrophs in deep-sea hydrothermal systems hosted in different rock types.
947 *Geochim Cosmochim Acta* 75:5736–5748.
948 8. Fortunato CS, Huber JA. 2016. Coupled RNA-SIP and metatranscriptomics of active
949 chemolithoautotrophic communities at a deep-sea hydrothermal vent. *ISME J* 10:1925–1938.
950 9. Olins HC, Rogers DR, Preston C, Ussler W 3rd, Pargett D, Jensen S, Roman B, Birch JM,
951 Scholin CA, Haroon MF, Girguis PR. 2017. Co-registered Geochemistry and
952 Metatranscriptomics Reveal Unexpected Distributions of Microbial Activity within a
953 Hydrothermal Vent Field. *Front Microbiol* 8:1042.

10. Fortunato CS, Larson B, Butterfield DA, Huber JA. 2018. Spatially distinct, temporally stable microbial populations mediate biogeochemical cycling at and below the seafloor in hydrothermal vent fluids. *Environ Microbiol* 20:769–784.

11. McNichol J, Stryhanyuk H, Sylva SP, Thomas F, Musat N, Seewald JS, Sievert SM. 2018. Primary productivity below the seafloor at deep-sea hot springs. *Proc Natl Acad Sci* 115:6756–6761.

12. Opatkiewicz AD, Butterfield DA, Baross JA. 2009. Individual hydrothermal vents at Axial Seamount harbor distinct subseafloor microbial communities. *FEMS Microbiol Ecol* 70:413–424.

13. Perner M, Bach W, Hentscher M, Koschinsky A, Garbe-Schönberg D, Streit WR, Strauss H. 2009. Short-term microbial and physico-chemical variability in low-temperature hydrothermal fluids near 5 degrees S on the Mid-Atlantic Ridge. *Environ Microbiol* 11:2526–2541.

14. Perner M, Hansen M, Seifert R, Strauss H, Koschinsky A, Petersen S. 2013. Linking geology, fluid chemistry, and microbial activity of basalt- and ultramafic-hosted deep-sea hydrothermal vent environments. *Geobiology* 11:340–355.

15. Huber JA, Mark Welch DB, Morrison HG, Huse SM, Neal PR, Butterfield DA, Sogin ML. 2007. Microbial population structures in the deep marine biosphere. *Science* 318:97–100.

16. Huber JA, Cantin HV, Huse SM, Welch DBM, Sogin ML, Butterfield DA. 2010. Isolated communities of Epsilonproteobacteria in hydrothermal vent fluids of the Mariana Arc seamounts. *FEMS Microbiol Ecol* 73:538–549.

17. Akerman NH, Butterfield DA, Huber JA. 2013. Phylogenetic diversity and functional gene patterns of sulfur-oxidizing subseafloor Epsilonproteobacteria in diffuse hydrothermal vent fluids. *Front Microbiol* 4:185.

18. Larson BI, Houghton JL, Lowell RP, Farough A, Meile CD. 2015. Subsurface conditions in hydrothermal vents inferred from diffuse flow composition, and models of reaction and transport. *Earth Planet Sci Lett* 424:245–255.

19. Meier D. 2016. PhD Thesis. University of Bremen, Bremen, Germany. Bacterial niche adaptation at hydrothermal vents.

20. Reveillaud J, Reddington E, McDermott J, Algar C, Meyer JL, Sylva S, Seewald J, German CR, Huber JA. 2016. Subseafloor microbial communities in hydrogen-rich vent fluids from hydrothermal systems along the Mid-Cayman Rise. *Environ Microbiol* 18:1970–1987.

21. Galambos D, Anderson RE, Reveillaud J, Huber JA. 2019. Genome-resolved metagenomics and metatranscriptomics reveal niche differentiation in functionally redundant microbial communities at deep-sea hydrothermal vents. *Environ Microbiol* 21:4395–4410.

22. Fullerton H, Smith L, Enriquez A, Butterfield D, Wheat CG, Moyer CL. 2024. Seafloor incubation experiments at deep-sea hydrothermal vents reveal distinct biogeographic signatures of autotrophic communities. *FEMS Microbiol Ecol* 100.

23. Fortunato CS, Butterfield DA, Larson B, Lawrence-Slavas N, Algar CK, Zeigler Allen L, Holden JF, Proskurowski G, Reddington E, Stewart LC, Topçuoğlu BD, Vallino JJ, Huber JA. 2021. Seafloor incubation experiment with deep-sea hydrothermal vent fluid reveals effect of pressure and lag time on autotrophic microbial communities. *Appl Environ Microbiol* 87.

24. Trembath-Reichert E, Butterfield DA, Huber JA. 2019. Active subseafloor microbial communities from Mariana back-arc venting fluids share metabolic strategies across different thermal niches and taxa. *ISME J* 13:2264–2279.

998 25. Lueders T. 2010. Stable isotope probing of hydrocarbon-degraders. p 4011–4026. In Timmis
999 KN (ed), Handbook of Hydrocarbon and Lipid Microbiology. Springer, Berlin.
1000 https://doi.org/10.1007/978-3-540-77587-4_312
1001 26. Lueders T, Dumont MG, Bradford L, Manefield M. 2016. RNA-stable isotope probing: from
1002 carbon flow within key microbiota to targeted transcriptomes. *Curr Opin Biotechnol* 41:83–
1003 89.
1004 27. Butterfield DA, Roe KK, Lilley MD, Huber JA, Baross JA, Embley RW, Massoth GJ. 2004.
1005 Mixing, reaction and microbial activity in the sub-seafloor revealed by temporal and spatial
1006 variation in diffuse flow vents at Axial Volcano. *In* The Subseafloor Biosphere at Mid-Ocean
1007 Ridges 144:269–289.
1008 28. Stewart LC, Algar CK, Fortunato CS, Larson BI, Vallino JJ, Huber JA, Butterfield DA, Holden
1009 JF. 2019. Fluid geochemistry, local hydrology, and metabolic activity define methanogen
1010 community size and composition in deep-sea hydrothermal vents. *ISME J* 13:1711–1721
1011 29. Zhou Z, Tran PQ, Cowley ES, Trembath-Reichert E, Anantharaman K. 2024. Diversity and
1012 ecology of microbial sulfur metabolism. *Nat Rev Microbiol* 23:122–140.
1013 30. Takai K, Campbell BJ, Cary SC, Suzuki M, Oida H, Nunoura T, Hirayama H, Nakagawa S,
1014 Suzuki Y, Inagaki F, Horikoshi K. 2005. Enzymatic and genetic characterization of carbon and
1015 energy metabolisms by deep-sea hydrothermal chemolithoautotrophic isolates of
1016 Epsilonproteobacteria. *Appl Environ Microbiol* 71:7310–7320.
1017 31. Nakagawa S, Takai K. 2008. Deep-sea vent chemoautotrophs: diversity, biochemistry and
1018 ecological significance: Chemoautotrophy in deep-sea vents. *FEMS Microbiol Ecol* 65:1–14.

1019 32. Nübel T, Klughammer C, Huber R, Hauska G, Schütz M. 2000. Sulfide:quinone
1020 oxidoreductase in membranes of the hyperthermophilic bacterium Aquifex aeolicus (VF5).
1021 *Arch Microbiol* 173:233–244.
1022 33. Perner M, Hentscher M, Rychlik N, Seifert R, Strauss H, Bach W. 2011. Driving forces behind
1023 the biotope structures in two low-temperature hydrothermal venting sites on the southern Mid-
1024 Atlantic Ridge: Driving forces behind vent biotopes. *Environ Microbiol Rep* 3:727–737.
1025 34. Nishimura H, Kitano Y, Inoue T, Nomura K, Sako Y. 2010. Purification and characterization
1026 of membrane-associated hydrogenase from the deep-sea epsilonproteobacterium
1027 Hydrogenimonas thermophila. *Biosci Biotechnol Biochem* 74:1624–1630.
1028 35. Campbell BJ, Smith JL, Hanson TE, Klotz MG, Stein LY, Lee CK, Wu D, Robinson JM,
1029 Khouri HM, Eisen JA, Cary SC. 2009. Adaptations to submarine hydrothermal environments
1030 exemplified by the genome of Nautilia profundicola. *PLoS* Genet 5:e1000362.
1031 36. Kubik BC, Holden JF. 2024. Non-thermodynamic factors affect competition between
1032 thermophilic chemolithoautotrophs from deep-sea hydrothermal vents. *Appl Environ*
1033 *Microbiol* 90:e0029224.
1034 37. Stewart LC. 2015. PhD thesis. University of Massachusetts Amherst, Amherst, MA. Energetic
1035 Limitations of Thermophilic Methanogens And Thiosulfate Reducers in The Subsurface
1036 Biosphere at Deep-Sea Hydrothermal Vents.
1037 38. Stewart LC, Llewellyn JG, Butterfield DA, Lilley MD, Holden JF. 2016. Hydrogen and
1038 thiosulfate limits for growth of a thermophilic, autotrophic Desulfurobacterium species from a
1039 deep-sea hydrothermal vent. *Environ Microbiol Rep* 8:196–200.

1040 39. Kristjansson JK, Schönheit P, Thauer RK. 1982. Different K_s values for hydrogen of
1041 methanogenic bacteria and sulfate reducing bacteria: An explanation for the apparent inhibition
1042 of methanogenesis by sulfate. *Arch Microbiol* 131:278–282.
1043 40. Lovley DR, Dwyer DF, Klug MJ. 1982. Kinetic analysis of competition between sulfate
1044 reducers and methanogens for hydrogen in sediments. *Appl Environ Microbiol* 43:1373–1379.
1045 41. Robinson JA, Tiedje JM. 1984. Competition between sulfate-reducing and methanogenic
1046 bacteria for H_2 under resting and growing conditions. *Arch Microbiol* 137:26–32.
1047 42. Ver Eecke HC, Butterfield DA, Huber JA, Lilley MD, Olson EJ, Roe KK, Evans LJ, Merkel
1048 AY, Cantin HV, Holden JF. 2012. Hydrogen-limited growth of hyperthermophilic
1049 methanogens at deep-sea hydrothermal vents. *Proc Natl Acad Sci* 109:13674–13679.
1050 43. Takai K, Nealson KH, Horikoshi K. 2004. Hydrogenimonas thermophila gen. nov., sp. nov., a
1051 novel thermophilic, hydrogen-oxidizing chemolithoautotroph within the epsilon-
1052 Proteobacteria, isolated from a black smoker in a Central Indian Ridge hydrothermal field. *Int*
1053 *J Syst Evol Microbiol* 54:25–32.
1054 44. Campbell BJ, Engel AS, Porter ML, Takai K. 2006. The versatile epsilon-proteobacteria: key
1055 players in sulphidic habitats. *Nat Rev Microbiol* 4:458–468.
1056 45. Sievert SM, Hügler M, Taylor CD, Wirsen CO. 2008. Sulfur oxidation at deep-sea
1057 hydrothermal vents, p. 238–258. *In* Microbial Sulfur Metabolism. Springer Berlin Heidelberg,
1058 Berlin, Heidelberg.
1059 46. Wommack KE, Williamson SJ, Sundbergh A, Helton RR, Glazer BT, Portune K, Craig Cary
1060 S. 2004. An instrument for collecting discrete large-volume water samples suitable for
1061 ecological studies of microorganisms. *Deep Sea Res Part I* 51:1781–1792.

1062 47. Bolger AM, Lohse M, Usadel B. 2014. Trimmomatic: a flexible trimmer for Illumina sequence
1063 data. *Bioinformatics* 30:2114–2120.
1064 48. Lo C-C, Chain PSG. 2014. Rapid evaluation and quality control of next generation
1065 sequencing data with FaQCs. BMC Bioinformatics 15:366.
1066 49. Ewels P, Magnusson M, Lundin S, Käller M. 2016. MultiQC: summarize analysis results for
1067 multiple tools and samples in a single report. *Bioinformatics* 32:3047–3048.
1068 50. Peng Y, Leung HCM, Yiu SM, Chin FYL. 2012. IDBA-UD: a de novo assembler for single-
1069 cell and metagenomic sequencing data with highly uneven depth. *Bioinformatic*s 28:1420–
1070 1428.
1071 51. Mikheenko A, Saveliev V, Gurevich A. 2016. MetaQUAST: evaluation of metagenome
1072 assemblies. *Bioinformatics* 32:1088–1090.
1073 52. Bray NL, Pimentel H, Melsted P, Pachter L. 2016. Near-optimal probabilistic RNA-seq
1074 quantification. *Nat Biotechno*l 34:888.
1075 53. Li D, Liu C-M, Luo R, Sadakane K, Lam T-W. 2015. MEGAHIT: an ultra-fast single-node
1076 solution for large and complex metagenomics assembly via succinct de Bruijn graph.
1077 *Bioinformatics* 31:1674–1676.
1078 54. Kang DD, Li F, Kirton E, Thomas A, Egan R, An H, Wang Z. 2019. MetaBAT 2: an adaptive
1079 binning algorithm for robust and efficient genome reconstruction from metagenome
1080 assemblies. *PeerJ* 7:e7359.
1081 55. Li H. 2013. Aligning sequence reads, clone sequences and assembly contigs with BWA-MEM.
1082 *arXiv*.

1083 56. Li H, Handsaker B, Wysoker A, Fennell T, Ruan J, Homer N, Marth G, Abecasis G, Durbin
1084 R, 1000 Genome Project Data Processing Subgroup. 2009. The Sequence Alignment/Map
1085 format and SAMtools. *Bioinformatics* 25:2078–2079.
1086 57. Sieber CMK, Probst AJ, Sharrar A, Thomas BC, Hess M, Tringe SG, Banfield JF. 2018.
1087 Recovery of genomes from metagenomes via a dereplication, aggregation and scoring strategy.
1088 *Nat Microbio*l 3:836–843.
1089 58. Chaumeil P-A, Mussig AJ, Hugenholtz P, Parks DH. 2022. GTDB-Tk v2: memory friendly
1090 classification with the genome taxonomy database. *Bioinformatics* 38:5315–5316.
1091 59. Magoč T, Salzberg SL. 2011. FLASH: fast length adjustment of short reads to improve genome
1092 assemblies. *Bioinformatics* 27:2957–2963.
1093 60. Kopylova E, Noé L, Touzet H. 2012. SortMeRNA: fast and accurate filtering of ribosomal
1094 RNAs in metatranscriptomic data. *Bioinformatics* 28:3211–3217.
1095 61. Schloss PD, Westcott SL, Ryabin T, Hall JR, Hartmann M, Hollister EB, Lesniewski RA,
1096 Oakley BB, Parks DH, Robinson CJ, Sahl JW, Stres B, Thallinger GG, Van Horn DJ, Weber
1097 CF. 2009. Introducing mothur: open-source, platform-independent, community-supported
1098 software for describing and comparing microbial communities. *Appl Environ Microbiol*
1099 75:7537–7541.
1100 62. Soneson C, Love MI, Robinson MD. 2015. Differential analyses for RNA-seq: transcript-level
1101 estimates improve gene-level inferences. F1000Res 4:1521.
1102 63. Love MI, Huber W, Anders S. 2014. Moderated estimation of fold change and dispersion for
1103 RNA-seq data with DESeq2. *Genome Biol* 15:550.

1104 64. Takahashi S, Tomita J, Nishioka K, Hisada T, Nishijima M. 2014. Development of a
1105 prokaryotic universal primer for simultaneous analysis of Bacteria and Archaea using next-
1106 generation sequencing. *PLoS One* 9:e105592.
1107 65. Crump BC, Kling GW, Bahr M, Hobbie JE. 2003. Bacterioplankton community shifts in an
1108 arctic lake correlate with seasonal changes in organic matter source. *Appl Environ Microbiol*
1109 69:2253–2268.
1110 66. Zhou J, Bruns MA, Tiedje JM. 1996. DNA recovery from soils of diverse composition. *Appl*
1111 *Environ Microbiol 62*:316–322.
1112

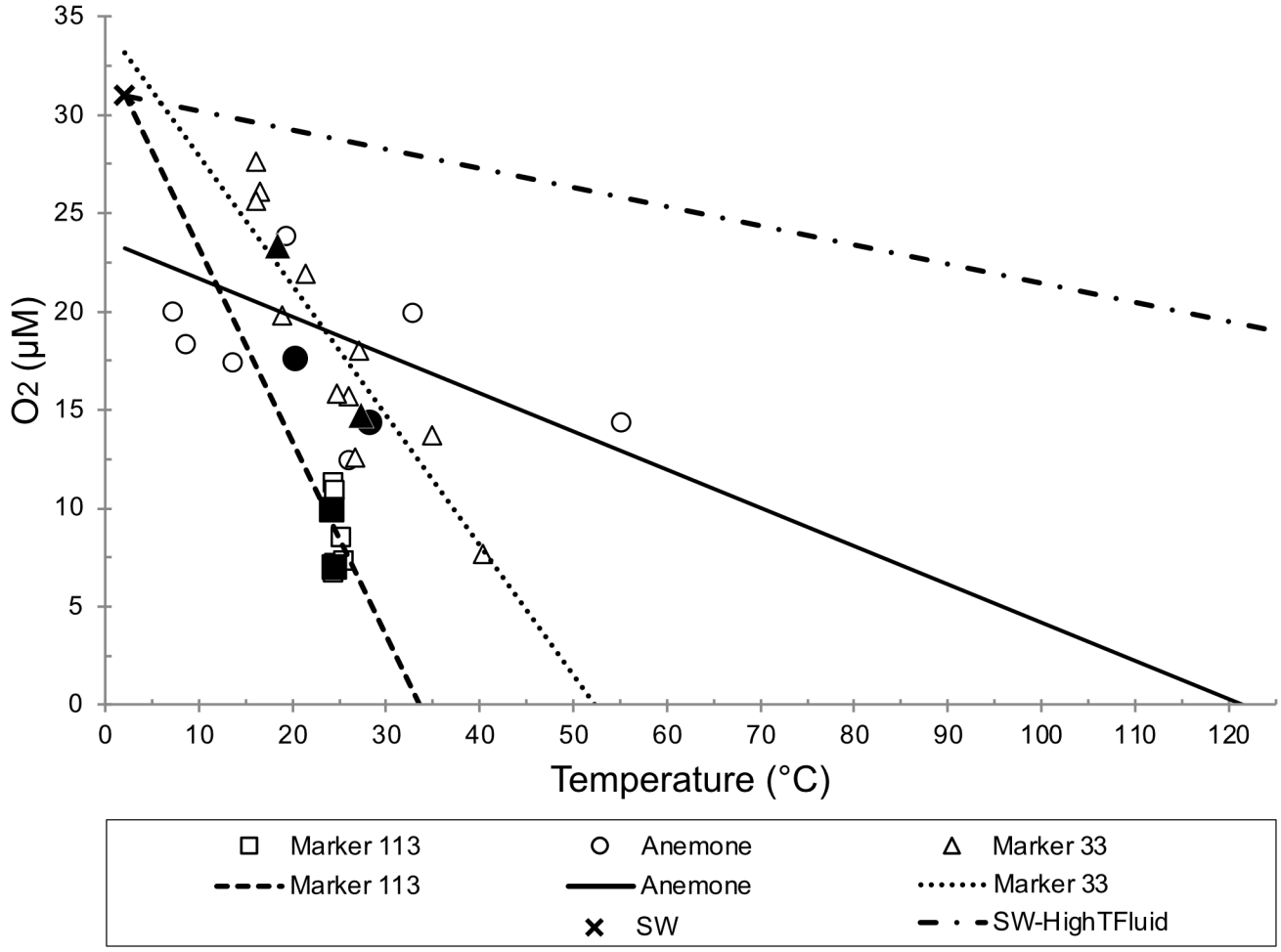
35
30
25
20
15
10
5
0
O2 (µM)
0
10
20
30
40
50
60
70
80
90
100
110
120
Temperature (°C)
Marker 113
Anemone
Marker 33
Marker 113
Anemone
Marker 33
SW
SW-HighTFluid

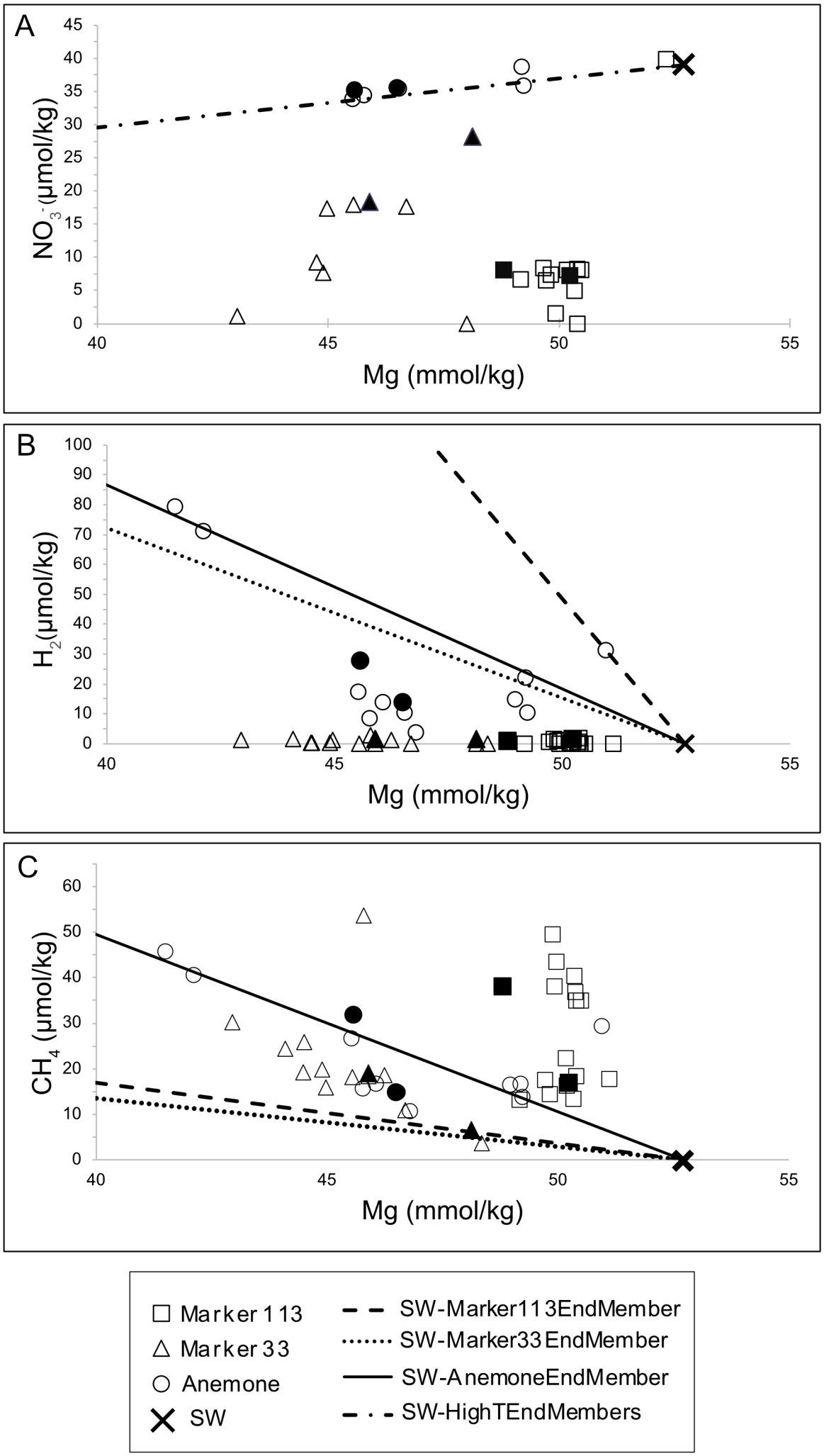
A
NO_3^- (µmol/kg)
Mg (mmol/kg)
B
H_2(µmol/kg)
Mg (mmol/kg)
C
CH_4 (µmol/kg)
Mg (mmol/kg)
Marker 113
Marker 33
Anemone
SW
SW-Marker113EndMember
SW-Marker33EndMember
SW-AnemoneEndMember
SW-HighTEndMembers

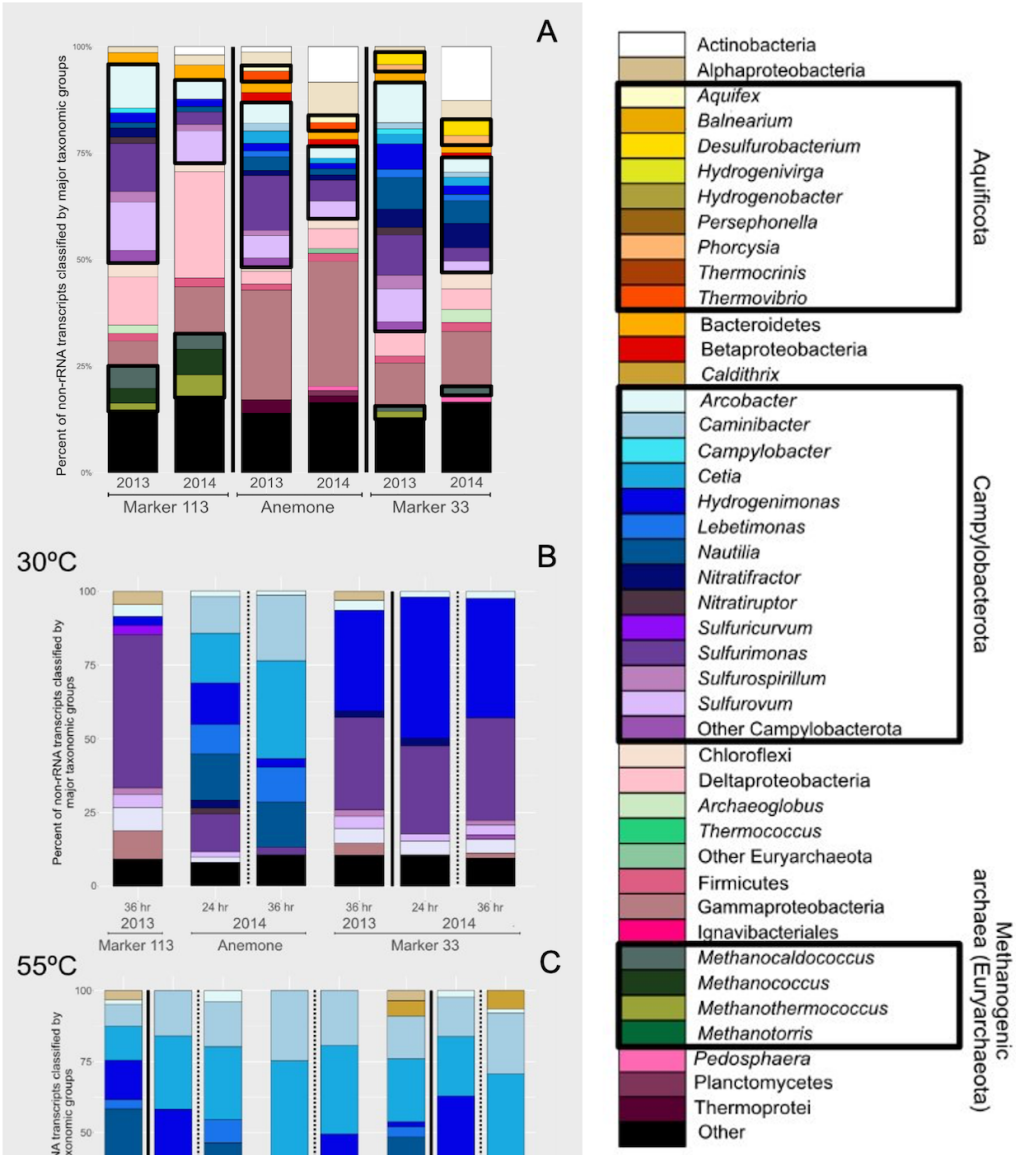
A
Percent of non-rRNA transcripts classified by major taxonomic groups
100%
75%
50%
25%
0%
2013
2014
2013
2014
2013
2014
Marker 113
Anemone
Marker 33
30ºC
B
Percent of non-rRNA transcripts classified by major taxonomic groups
100
75
50
25
0
36 hr
24 hr
36 hr
36 hr
24 hr
36 hr
2013
2014
2013
2014
Marker 113
Anemone
Marker 33
55ºC
C
Percent of non-rRNA transcripts classified by major taxonomic groups
100
75
50
25
0
36 hr
18 hr
36 hr
18 hr
36 hr
36 hr
18 hr
36 hr
2013
2014
2014
2013
2014
Marker 113
Anemone
Marker 33
80ºC
D
Percent of non-rRNA transcripts classified by major taxonomic groups
100
75
50
25
0
18 hr
9 hr
18 hr
18 hr
36 hr
9 hr
18 hr
2013
2014
2013
2014
2013
2014
Marker 113
Anemone
Marker 33
Actinobacteria
Alphaproteobacteria
Aquifex
Balnearium
Desulfurobacterium
Hydrogenivirga
Hydrogenobacter
Persephonella
Phorcysia
Thermocrinis
Thermovibrio
Aquificota
Bacteroidetes
Betaproteobacteria
Caldithrix
Arcobacter
Caminibacter
Campylobacter
Cetia
Hydrogenimonas
Lebetimonas
Nautilia
Nitratifractor
Nitratiruptor
Sulfuricurvum
Sulfurimonas
Sulfurospirillum
Sulfurovum
Other Campylobacterota
Campylobacterota
Chloroflexi
Deltaproteobacteria
Archaeoglobus
Thermococcus
Other Euryarchaeota
Firmicutes
Gammaproteobacteria
Ignavibacteriales
Methanocaldococcus
Methanococcus
Methanothermococcus
Methanotorris
Methanogenic archaea (Euryarchaeota)
Pedosphaera
Planctomycetes
Thermoprotei
Other

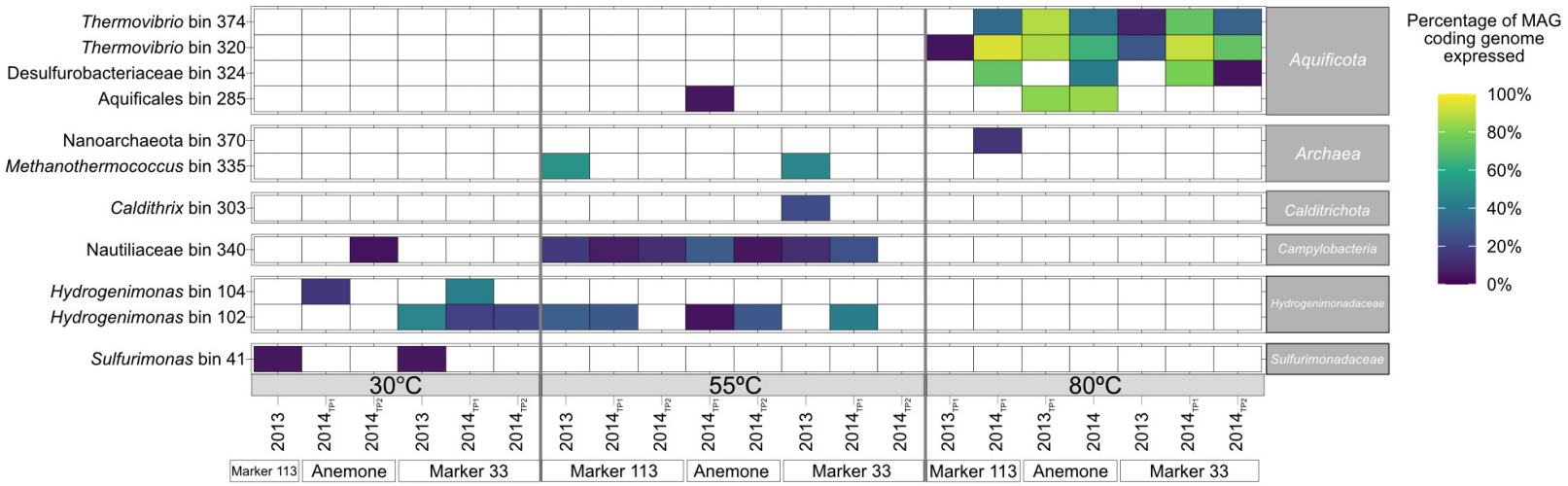
Thermovibrio bin 374
Thermovibrio bin 320
Desulfurobacteriaceae bin 324
Aquificales bin 285
Nanoarchaeota bin 370
Methanothermococcus bin 335
Caldithrix bin 303
Nautiliaceae bin 340
Hydrogenimonas bin 104
Hydrogenimonas bin 102
Sulfurimonas bin 41
Aquificota
Archaea
Calditrichota
Campylobacteria
Hydrogenimonadaceae
Sulfurimonadaceae
30°C
55ºC
80ºC
2013
2014TP1
2014TP2
2013TP1
Marker 113
Anemone
Marker 33
Percentage of MAG coding genome expressed
100%
80%
60%
40%
20%
0%

Normalized abundance of transcripts
0
11000
22000
33000
44000
55000
66000
Oxygen
Nitrogen
Sulfur
Methane
Hydrogen
Carbon
Cytochrome c oxidase cbb3-type (ccoNOPQ)
Cytochrome c oxidase, aa3-type (coxABCD)
Dissimilatory nitrite reductase (nirB, nrfA)
Nitrate reductase/nitrite oxidoreductase (narG, narZ, nxrA)
Ferredoxin-nitrite reductase (nirA)
Periplasmic nitrate reductase (napAB)
Nitrite reductase (nirSK)
Nitric oxide reductase (norBC)
Nitrous oxide reductase (nosZ)
Polysulfide/thiosulfate reductase (psrAC, phsAC)
Sulfite reductase (dsrAB)
Adenylylsulfate reductase (aprAB)
Sulfur oxidizing protein (soxABCDXYZ)
Sulfide:quinone oxidoreductase (sqr)
Sulfate adenylyltransferase (sat, met3)
CoB-CoM heterodisulfide reductase (hdrA2BC)
Formylmethanofuran dehydrogenase subunit B (fwdB, fmdB)
Acetyl-CoA decarbonylase/synthase complex (cdhACDE)
Coenzyme F420 hydrogenase (frhABDG)
Tetrahydromethanopterin S-methyltransferase (mtrABCDEFGH)
Methyl coenzyme M reductase (mcrABCDG)
Sulfhydrogenase (hydABDG)
Quinone-reactive Ni-Fe hydrogenase, group 1 (hydAB)
Ni-Fe Hydrogenase, group 1 (hyaABCD, hybCDO)
F420-non-reducing hydrogenase (mvhADG, vhuADG, vhcADG)
Ech hydrogenase (echABCDEF)
2-oxoglutarate/2-oxoacid ferredoxin oxidoreductase
(TCA cycle, Reductive TCA cycle, korA, oorA, oforA)
Isocitrate dehydrogenase
(TCA cycle, Reductive TCA cycle, IDH1, IDH2, icd)
ATP-citrate lyase (Reductive TCA cycle, aclAB)
Anaerobic carbon-monoxide dehydrogenase
(Wood-Ljundahl pathway, cooS, acsA)
Ribulose-bisphosphate carboxylase (CBB cycle, rbcSL, cbbL)
MetaT
30°C
55°C
80°C
TP1
TP2
2013
2014
Marker 113
Anemone
Marker 33

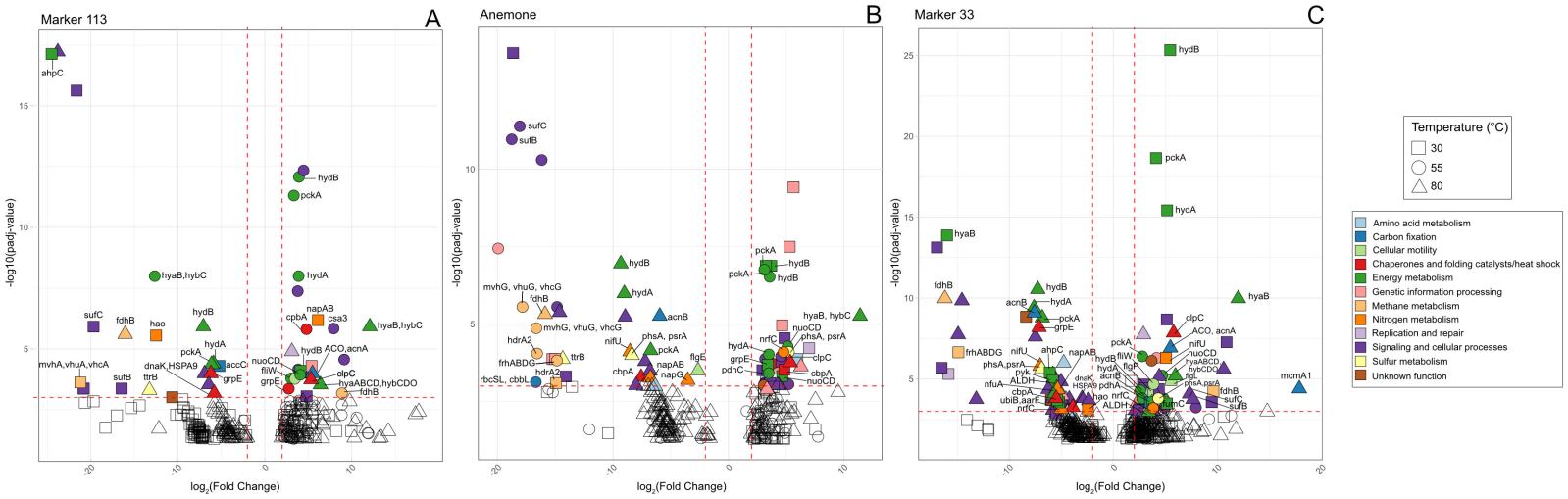
Marker 113
A
Anemone
B
Marker 33
C
-log10(padj-value)
log2(Fold Change)
Temperature (°C)
30
55
80
Amino acid metabolism
Carbon fixation
Cellular motility
Chaperones and folding catalysts/heat shock
Energy metabolism
Genetic information processing
Methane metabolism
Nitrogen metabolism
Replication and repair
Signaling and cellular processes
Sulfur metabolism
Unknown function

	Seawater	Anemone high-temperature vent	Anemone diffuse vent	Anemone diffuse vent	Marker 33 Sub-seafloor estimated source	Marker 33 diffuse vent	Marker 33 diffuse vent	Marker 113 sub-seafloor estimated source	Marker 113 diffuse vent	Marker 113 diffuse vent
Year	2015	2013		2014		2013	2014		2013	2014
Depth (m)	1520	1542.8	1542	1539		1516	1514		1520	1518
Temperature (°C)	2	232.4	28.2	20.3	340	27.3	18.5	340	24.5	24.3
pH	7.8	4.3	5.5	5.1	4	5.5	5.6	3.3	6.2	5.8
NO_3^- (µmol/kg)	39	0	35.5	35.2	0	18.3	28.2	0	7.2	8.1
H_2 (µmol/kg)	0.002	360	13.9	27.7	300	1.5	1.5	950	1.4	1
H_2S (µmol/kg)	0	7400	1036	964.7	n.d.	545	262	n.d.	729	556
CH_4 (µmol/kg)	0.002	205	14.8	31.7	70	19	6.4	56	16.9	38
Mg (mmol/kg)	52.4	0	46.5	45.6	0	45.9	48.1	0	50.2	48.8
O_2 (µmol/L)	31	0	14.4	17.6	0	14.7	23.3	0	7	9.9
Cl^- (µmol/L)	541	315	513	518	390	520	526	100	521	518
Percent Seawater	100	3.3	88.9	87	0	87.7	91.9	0	96	96.4
Microbial cells mL^{-1}	2.4×10^4		4.1×10^5	1.7×10^5		4.2×10^5	3.9×10^5		4.6×10^5	6.8×10^5

Vent	Year	30 °C	55 °C	80 °C
Marker 113	2013	36 hr	36 hr	18 hr*
Marker 113	2014	n.d.	18 hr, 36 hr	9 hr
Anemone	2013	n.d.	n.d.	18 hr*
Anemone	2014	24 hr, 36 hr	18 hr, 36 hr	18 hr
Marker 33	2013	36 hr	36 hr	36 hr
Marker 33	2014	24 hr, 36 hr	18 hr, 36 hr	9 hr, 18 hr